Cooperative Trajectory Planning and Resource Allocation for UAV-enabled Integrated Sensing and Communication Systems

Yu Pan, Ruoguang Li, *Member, IEEE,* Xinyu Da, Hang Hu, Miao Zhang, *Member, IEEE,* Dong Zhai, Kanapathippillai Cumanan, *Senior Member, IEEE,* and Octavia A. Dobre, *Fellow, IEEE*

***Abstract*—The flexibility and controllable mobility of unmanned aerial vehicles (UAVs) render them easier to become aerial platforms carrying out integrated sensing and communication (ISAC) functionality, and the cooperation among multiple UAVs is a promising way to achieve simultaneous multi-static radar sensing and coordinated multiple point (CoMP) transmission, leading to an enhanced ISAC service. However, due to the intrinsically limited resources that UAVs can utilize, it is challenging to achieve performance improvement for dual purposes. Toward this end, in this paper, an orthogonal frequency division multiple access (OFDMA) UAV-enabled ISAC system is investigated, and a joint trajectory planning and resource allocation problem is formulated to minimize the Cramér-Rao lower bounds (CRLB) for target location estimation while guaranteeing the communication quality-of-service (QoS) constraints. The formulated problem is non-convex and difficult to solve in general, and we first decompose the original problem into three sub-problems and then propose the corresponding algorithms to obtain the optimal solutions efficiently. The extensive simulations demonstrate the convergence of the proposed algorithm and the performance improvement on the localization with different communication requirements compared to conventional techniques.**

***Index Terms*—Integrated sensing and communications (ISAC), cooperative unmanned aerial vehicle (UAV) network, trajectory planning, resource allocation**

This work was supported in part by the National Natural Science Foundation of China under Grant No. 62371131 and No. 62101080, in part by the Natural Science Foundation of Jiangsu Province of China under Grant No. BK20230823, in part by the Chongqing Municipal Education Commission under Grant No. KJQN202100738 and in part by the Chongqing Science and Technology Bureau under Grant No. CSTB2022BSXM-JCX0113. The work of K. Cumanan was supported by the UK Engineering and Physical Sciences Research Council (EPSRC) under grant number EP/X01309X/1, and the work of O. A. Dobre was supported by the Natural Sciences and Engineering research Council of Canada (NSERC) through its Discovery program. *(Corresponding author: Ruoguang Li.)*

Y. Pan is with the School of Electronic Countermeasures, National University of Defense Technology, Hefei 230037, China (e-mail: panyu@mail.nwpu.edu.cn).

R. Li is with the National Mobile Communications Research Laboratory, Southeast University, Nanjing 210096, China (email: ruoguangli@seu.edu.cn).

X. Da is with the College of Artificial Intelligence, Yango University, Fuzhou 350015, China (e-mail: kgddxy@163.com).

H. Hu is with the Information and Navigation College, Air Force Engineering University, Xi'an 710077, China (e-mail: xd_huhang@126.com).

M. Zhang is with the School of Information Science and Engineering, Chongqing Jiaotong University, Chongqing 400074, China, (email: msczz@foxmail.com).

D. Zhai is with the Equipment Management and Unmanned Aerial Vehicle Engineering School, Air Force Engineering University, Xi'an 710077, China (e-mail: zhaidongwzwdl@163.com).

K. Cumanan is with the School of Physics, Engineering and Technology, University of York, York, United Kingdom, YO10 5DD (email: kanapathippillai.cumanan@york.ac.uk).

Octavia A. Dobre is with the Department of Electrical and Computer Engineering, Memorial University, St. Johns, NL A1B 3X5, Canada (e-mail: odobre@mun.ca).

I. Introduction

A. Background and Motivations

In recent years, integrating unmanned aerial vehicles (UAVs) into the sixth-generation (6G) communication system cellular networks has been continuously researched and developed [1]. These techniques have been applied in numerous scenarios, such as intelligent transportation, environmental monitoring disaster relief, etc [2]. Due to its maneuverability, intelligence, high flexibility, and ubiquitous coverage [3], UAVs can complete various dangerous tasks without the involvement of human beings at a low cost bringing wide prospects in civil and military applications.

The potential applications of the 6G mobile systems include smart transportation and cities, which introduce more stringent communication and sensing demands. For example, the communication requires ultra-low latency and high reliability [4], whereas the sensing requires high precision and resolution [5]. The realization of the 6G vision necessitates an architecture that is capable of deeply integrating perceptual information acquisition, information sharing, intelligent data processing, and control instruction distribution among the users. Specifically, in UAV networks, wireless sensing is the primary demand for surveillance, illegitimate target detection, and collision avoidance. In addition, high-quality communication services among UAVs, base stations (BSs), and users are also necessary. Therefore, sensing and communication are two key technologies for exploring future use-cases and emerging applications, while the continuous development of UAV technology will put forward demanding requirements for both functionalities. However, conventional radar sensing and communication modules are individually designed in fully separate spectrum and transceivers, which are undoubtedly expensive and restricted in resource utilization, although the spectrum resources are particularly scarce.

Exploiting integrated sensing and communication (ISAC) technology with shared signal and transceivers is one approach to compensate for the above-mentioned limitations, which can achieve load-saving and spectrum-reusing [6]. The unified transceivers can be built using light-weight wireless equipment with both communication and sensing functionalities, while the shared spectrum can improve spectrum utilization [7], [8]. Due to the high altitude, UAVs can achieve wider coverage areas with a high probability of line-of-sight (LoS) links. Therefore, exploiting UAV in the ISAC system can eliminate the performance degradation of communication and

sensing/localization in urban or mountainous forest scenarios. Mobile sensor networks are known to offer distinctive advantages over terrestrial networks in terms of sensing coverage [9], adaptability to changing conditions, and robustness against failures [10]. Therefore, multiple UAVs can cooperatively perform an aerial distributed radar sensing and wireless communication network, realizing the function of multi-static radar and coordinated multi-point joint transmission (CoMP-JT), which makes it possible to further enhance the sensing and communication performance [11]. Furthermore, this combination can promote the realization of global coverage and ubiquitous connectivity for 6G, by expanding the system capability from a traditional two-dimensional ground network to three-dimensional space-air-ground network coverage [12], and from traditional communication capacity to dual function radar and communication (DFRC) capacity. Intuitively, the more transmit resource is utilized to serve multiple users, the better sensing and communication quality-of-service (QoS) will be obtained. Unfortunately, resources (e.g., transmit power, bandwidth, etc.) are always limited for practical applications, resulting in the demand for performance trade-off among the users. To that end, efficient resource allocation schemes are necessary to achieve optimal QoS performance.

B. Related Works

An overview of ISAC towards 6G has been summarized comprehensively in [6], where the existing dual-functional waveforms are mainly designed from two perspectives: embedding useful information into radar signals and employing the existing communication signals for radar detection [13]. As a promising communication-centric waveform for ISAC, orthogonal frequency division multiplexing (OFDM) has been extensively investigated for the ISAC design in [14] and [15]. OFDM was initially suited for communication since it can provide robustness against multipath fading and facilitate adaptive modulation, and its estimation performance has been validated by theory and experimental measurements to be as accurate as frequency-modulated continuous wave (FMCW) in [16]-[17]. Several studies have been presented to enhance joint sensing and communication performance by optimizing the OFDM parameters [18]-[21]. For example, for the OFDM-ISAC system incorporating specifications-compliant transmission waveforms based on 3GPP long-term evolution (LTE), the impact of unused subcarriers within the transmitted signal passband, the fundamental hardware challenges related to transmitter-receiver isolation, and associated self-interference problem were addressed in [18]. In [19], the OFDM waveform matrix was designed to improve the channel capacity and radar detection performance in the proposed RadCom architecture, while the authors considered the conditional mutual information and the data information rate in [20]. Moreover, [21] demonstrated that the theoretical lower bounds of the radar system's parameters of interest can be minimized by waveform optimization at the cost of reducing the power allocated for the communication subcarriers, where the radar transceiver and the communication transmitter are considered to be the same full-duplex BS. The expensive cost of fully digital beamforming architecture motivated the investigation of hybrid beamforming for the OFDM-ISAC system, to jointly optimize the spectral efficiency of communication and spatial spectrum matching error of radar [22].

As aforementioned, UAVs can be deployed quickly and easily as a cooperative mobile network to potentially enhance the communication and sensing abilities [23]. Many studies have focused on the performance enhancement in multi-UAV network from the perspective of communications [24]-[29] or sensing [31]-[37], separately. For communications, the placement, trajectory, and resource allocation of the UAVs can be jointly optimized to satisfy different quality-of-service (QoS) requirements. The effect of the UAV placement and path loss factor was analyzed in [25] for user coverage maximization in uplink transmission, while [26] focused on the power and time resource allocation problem for time sharing non-orthogonal multiple access UAV-assisted communications. In [27], the legitimate surveillance problem was investigated by optimizing the jamming power and 3D trajectory of the cooperative UAV in a maritime communication network, and two reinforcement learning schemes were further proposed in [28]. To fully utilize the advantages of UAV-enabled simultaneous wireless information and power transfer, [29] studied the system's robust joint design with imperfect eavesdropper locations to maximize the minimum secrecy rate under the harvested energy constraints, while the robust 3D-trajectory and time switching optimization was further investigated for a dual-UAV-enabled system in [30].

For radar sensing, to analyze the effect of radar geometric deployment on localization accuracy, the placement strategy of UAVs was considered for time of arrival (TOA)-based localization [31]-[32], and angle of arrival (AOA)-based localization [33] by using the Fisher information matrix (FIM) as the performance metric. In [34], a multi-UAV cooperative resource scheduling and task assignment scheme based on the animal colony perception method was proposed, providing a target recognition, location, and tracking method. To localize moving targets more efficiently, a cooperative path planning technique through predicting the FIM was presented in [35]. Furthermore, based on the map-aided estimator, the UAV trajectory was optimized in [36] to improve the performance of localization under a given mission duration. However, few works investigated the UAV-enabled ISAC system, which may introduce challenging problems in practice. In [37], a beam sharing scheme was proposed, and the corresponding beamforming algorithm to maximize the sensing range for each UAV was achieved. The joint UAV location problem was considered in a DFRC multi-UAV network to maximize the network utility in [23], and the UAV trajectory was optimized with a novel integrated periodic sensing and communication mechanism to maximize the user rate in [38]. However, the aforementioned works only considered UAVs' location optimization for performance enhancement, not mentioning the joint design problem of trajectory optimization and resource allocation with the QoS constraints yet, and thus motivates our current work on the trade-off between sensing and communication performance for an integrated waveform.

C. Original Contributions and Organization

In this paper, we study a UAV-enabled ISAC system, where multiple UAVs are employed to simultaneously provide sensing and communication services via the integrated waveform. In particular, the mean square error (MSE) of the location estimation is minimized under throughput constraints for each UAV, and then the cooperative trajectories and resource allocation are jointly optimized with limited power and spectrum resources. Such a resource-aware problem is non-trivial and practically appealing, and is beneficial in extending the ability of the ISAC system in terms of performance and endurance. However, this problem has not been investigated to the best of our knowledge. The variables of UAV trajectory, user association, transmission power, and bandwidth are coupled with each other and the problem is non-convex. After decomposition, the pattern search algorithm is first applied to determine the UAV tracking trajectories, and the Hungarian algorithm is utilized to solve the association problem. Toward this end, an alternative algorithm is proposed to iteratively obtain the optimal bandwidth allocation and power allocation with successive convex approximation (SCA) technique. The main contributions of this paper are summarized as follows.

- First, we propose a cooperative multi-UAV ISAC network to simultaneously provide target sensing and communication services. An OFDM-based waveform is adopted and the resource block allocation is proposed, and the ISAC framework and spectrum usage are elaborated.
- Then, to quantify the localization performance of the cooperative UAVs, equivalent FIM (EFIM) [39] is applied to directly calculate the FIM of ToA from each UAV, which can reduce the dimension of the determined FIM. Then, the Cramér-Rao lower bound (CRLB) for location estimation is derived as sensing performance criterion.
- The ranging performance of each UAV is analyzed to investigate the resource allocation principles, and the effects of the trajectory and resource allocation on the entire performance are accordingly demonstrated.
- Finally, we validate the effectiveness of the proposed *a*lternating *p*ath planning and *r*esource *a*llocation (APRA) algorithm by the theoretical results of CRLB. It is shown that the proposed algorithm is able to converge within few iterations and can significantly and efficiently improve the localization performance compared with conventional radar networks.

In the rest of this paper, Section II describes the system model, while Section III formulates the CRLB minimization problem under throughput constraints. In Section IV, the alternating algorithm is proposed to solve the non-convex problem, and Section V presents the simulation results and discussions. Finally, Section VI draws the conclusions.

Notations: Throughout the paper, matrices are denoted by bold upper-case letters (i.e., $\mathbf{\Lambda}$), column vectors are denoted by bold lower-case letters (i.e., $\mathbf{q}$), and scalars are denoted by normal letters (i.e., P). $|a|$ stands for the magnitude of a scalar a; diag$\{\boldsymbol{a}\}$ stands for a diagonal matrix with the elements of vector $\boldsymbol{a}$ on the diagonal. Matrix superscripts $(\cdot)^{\mathrm{T}}$ and $(\cdot)^{\mathrm{H}}$ represent the transpose and complex conjugate transpose operations, respectively. Besides, the notations $\mathrm{tr}(\cdot)$ and $(\cdot)^{-1}$ denote the trace and the inverse of a matrix.

II. System Model

A. System Description

As shown in Fig. 1, the system is consisted of K randomly distributed ISAC UAVs, one targeted UAV that is to be detected, and one fusion center (FC). The ISAC UAVs can perform simultaneous sensing and communication via the pre-designed ISAC waveform. The rotary-wing UAVs are deployed around the area of interest, and cruise at a fixed altitude to detect the malicious target while communicating with the BS. The locations of the unauthorized target, the k-th ISAC UAV, and the j-th BS at the i-th time interval are given by $\boldsymbol{\omega}^i \in \mathbb{R}^{2\times 1}$, $\mathbf{q}_k^i \in \mathbb{R}^{2\times 1}\,(k \in \mathcal{K} = \{1, \cdots, K\})$, and $\mathbf{u}_j \in \mathbb{R}^{2\times 1}\,(j \in \mathcal{J} = \{1, \cdots, J\})$, respectively. The FC not only manages the wireless resource scheduling among UAVs and BSs, but also collects the sensed results from each UAV for further processing. The synchronization among UAVs can be achieved by wireless backhaul links. Besides, the prior information of the coarse targeted UAV's location can be obtained by global positioning system (GPS). For ease of analysis, we assume that the clutter can be appropriately mitigated by using the existing clutter rejection techniques.

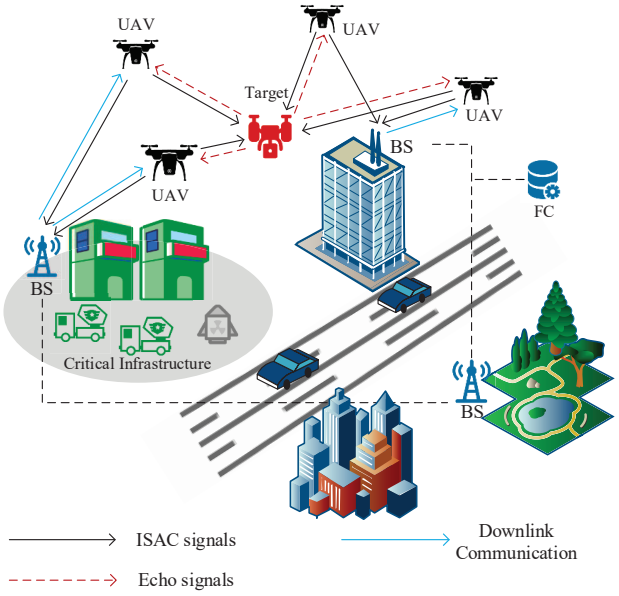

Fig. 1. A UAV-enabled ISAC system adopting OFDM.

The frame structure and schematic diagram for UAV-anbled ISAC system are described in Fig. 2, which is based on a typical time-division duplex (TDD) protocol. We assume that a time interval can be regarded as a slot for communication and a pulse repetition interval (PRI) for radar sensing[1]. As shown in Fig. 2(a), during the first time interval, all the UAVs transmit uplink pilots (UPs) to achieve target searching and uplink channel estimation, while BS transmits downlink polits

[1]Following the standard radar literature, a transmit-receive cycle is termed as a PRI [13].

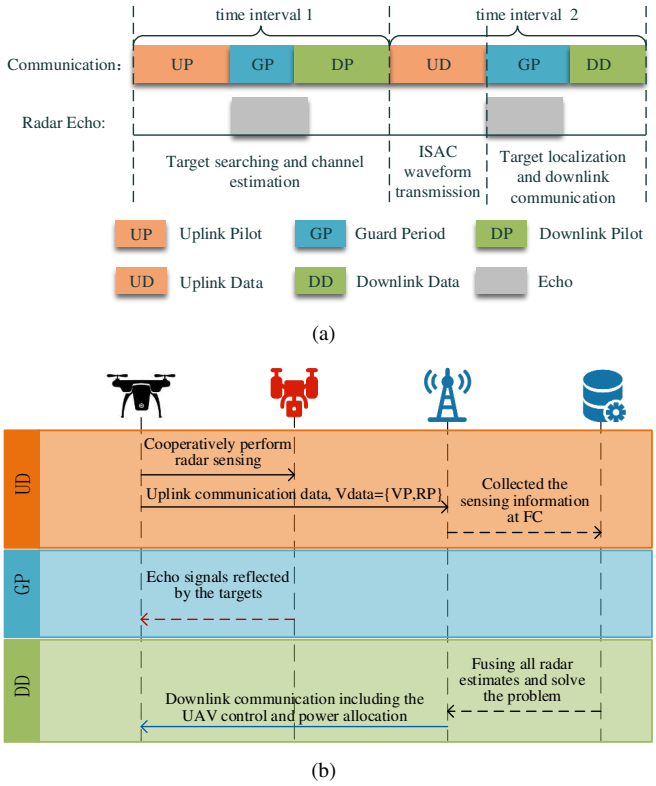

Fig. 2. (a) Frame structure of the ISAC signal; (b) Schematic diagram of the ISAC system in time interval 2.

(DPs) for downlink channel estimation. It is worth noting that a guard period (GP) is necessary to avoid the interference between downlink communications and echos. In the second time interval, UAVs transmit the ISAC waveform to perform simultaneous radar sensing and uplink data (UD) transmission[2] to the micro BSs. When the echo is reflected back from the target, the UAVs perform inner-measurement for ranging independently and then forward the processed result to the BSs by downlink data (DD), which will be finally collected at the FC. The TOA-based localization is considered in this paper for its easy deployment on UAV swarms, higher accuracy than received signal strength sensors, and lower complexity than the angle of departure and AOA sensors[3]. During the downlink communication, the BSs send the data including the solutions for trajectory control and resource allocation to each UAV, which is obtained from FC by fusing all ranging estimates.

The number of K ISAC UAVs communicate with the BSs via OFDM access (OFDMA), and the channel state information (CSI) is assumed to be perfectly known. The transmit power vector of the UAVs is denoted by $\mathbf{p}^i = [P_1^i, \cdots, P_K^i]^{\mathrm{T}}$, where P_k^i denotes the transmission power of the k-th UAV at the i-th interval. Without loss of generality, the OFDMA network is considered with N_c subcarriers to be allocated to K UAVs, and the spectrum usage is illustrated in Fig.3.

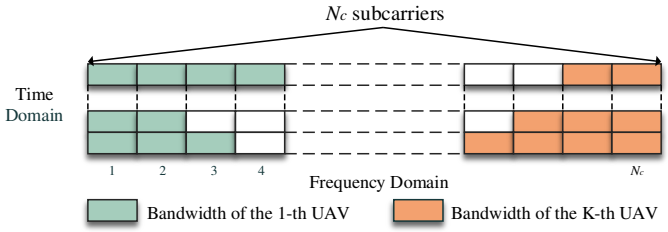

Fig. 3. The spectrum usage of the OFDMA network with N_c subcarriers for K UAVs.

Then, the OFDM-ISAC signal transmitted by the k-th UAV can be represented as [20]

$$S_k^i(t) = e^{\mathrm{j}2\pi f_{c,k} t} \sum_{n\in\mathcal{N}_k^i} \sum_{m=0}^{M-1} a_{kn}^i C_{k,nm}^i e^{\mathrm{j}2\pi n\Delta f(t-mT)} \times \mathrm{rect}\left[\frac{(t-mT)}{T}\right], \quad (1)$$

where $\mathcal{N}_k^i$ represents the assigned subcarrier set of the k-th UAV, M denotes the number of OFDM symbols in each pulse, a_{kn}^i is the amplitude of the n-th subcarrier of the k-th UAV with $P_k^i = \sum_{n\in\mathcal{N}_k^i} |a_{kn}^i|^2$, and $C_{k,nm}^i$ is the m-th modulated symbol on the n-th subcarrier. $\mathrm{rect}[t/T]$ is the rectangle function, and $\Delta f = 1/T$ is the subcarrier interval, where T is the length of each OFDM symbol composed of valid symbol time T_s and cyclic prefix (CP) time T_g. To avoid the inter-symbol interference (ISI), the length of CP must be larger than the maximum time delay of multi-path, while in radar systems T_g should also be larger than the round-trip time delay corresponding to the maximum detectable range.

B. Communication Model

The communication channel is mainly dependent on the propagation loss with respect to distance. Let h_{kj}^i denote the channel coefficient between the k-th UAV and the j-th BS at the i-th interval, which can be described by

$$h_{kj}^i = \sqrt{\gamma_{kj}^i}\tilde{h}_{kj}^i, \quad (2)$$

where γ_{kj}^i accounts for the large-scale fading effects, and $\tilde{h}_{kj}^i$ is a complex-valued random variable with $\mathbb{E}\left[\left|\tilde{h}_{kj}^i\right|^2\right] = 1$ accounting for the small-scale fading. Specifically, the large-scale fading effect varies based on LoS and Non line-of-sight (NLoS) link, which can be written as [40]

$$\gamma_{kj}^i = \begin{cases} \gamma_0 \left(d_{kj}^i\right)^{-\tilde{\alpha}}, & \text{LoS link} \\ \kappa\gamma_0 \left(d_{kj}^i\right)^{-\tilde{\alpha}}, & \text{NLoS link} \end{cases} \quad (3)$$

where γ_0 is the path loss at the reference distance, $\tilde{\alpha}$ is the path loss exponent, and $\kappa < 1$ is the additional attenuation factor due to the NLoS condition. Without loss of generality, we assume that each UAV experiences the same channel gain on each subcarrier due to smaller multipath effect in the air [41].

[2]The uplink communication data is defined as Vdata={VP, RP}, including VP={distance} for the target, and RP={detection picture/video} for environment and traffic status from the previous PRI, which are collected by wearable module embedded on the UAVs.

[3]It should be mentioned that our model is simplified for ease of analysis. And a more generalized model foe 3D localization needs to be considered in the future work.

The association between the UAV and BS at the i-th interval is denoted by an indicator matrix $\mathbf{\Lambda}^i \in \mathbb{R}^{K\times J}$, whose element at the k-th row and the j-th column is $\lambda_{kj} \in \{0,1\}$, where $\lambda_{kj} = 1$ indicates that the k-th UAV is associated with the j-th BS, and $\lambda_{kj} = 0$ otherwise. Since the UAVs communicate with the BSs via OFDMA, the mutual interference among downlinks is non-existent. We assume that each UAV can only communicate with one BS within each time interval, and each BS can serve N_a UAVs, then there exists

$$\begin{cases} \sum_{j\in\mathcal{J}} \lambda_{kj}^i = 1, & \forall k \in \mathcal{K}, \\ \sum_{k\in\mathcal{K}} \lambda_{kj}^i \le N_a, & \forall j \in \mathcal{J}. \end{cases} \tag{4}$$

Since channel capacity is a general and important criterion for communication, it is used as the metric to evaluate the communication performance in this ISAC system. The vector of subcarrier number allocation is denoted by $\mathbf{n}^i = [N_1^i, \cdots, N_K^i]^{\mathrm{T}}$, where N_k^i is the number of allocated subcarriers to the k-th UAV at the i-th interval, and thus its bandwidth is $B_k^i = N_k^i \Delta f$. The subcarriers can be allocated in consecutive or interleaved chunks to improve the frequency diversity. Therefore, the achievable rate of the k-th UAV at the i-th time interval can be obtained by

$$R_{c,k}^i = B_k^i \sum_{j\in\mathcal{J}} \lambda_{kj}^i \log_2 \left(1 + \frac{\left|a_{kn}^i h_{kj}^i\right|^2}{\sigma_{c,k}^2}\right), \tag{5}$$

where $\sigma_{c,k}^2$ is the noise power of the additive white Gaussian noise (AWGN) at the j-th BS, and the achievable sum rate is $R_c^i = \sum_{k\in\mathcal{K}} R_{c,k}^i$.

C. Localization Measurement Model

Once the echo is received by the k-th UAV, we can remove the echo from other UAVs since their status information are achievable at FC. Then the processed echo which only contains the information from the target can be formulated as

$$\begin{aligned} r_k^i(t) = \sum_{n\in\mathcal{N}_k^i} \sum_{m=0}^{M-1} \zeta_k^i a_{kn}^i C_{k,nm}^i e^{\mathrm{j}2\pi n\Delta f\left(t-mT-\tau_k^i\right)} \\ \times e^{\mathrm{j}2\pi[f_{c,k}\left(t-\tau_k^i\right)+f_{D,k}^i mT]} \operatorname{rect}\left[\frac{t-mT-\tau_k^i}{T}\right] + \phi_k(t), \end{aligned} \tag{6}$$

where $f_{c,kn} = f_{c,k} + n\Delta f$, and ζ_k^i denotes the complex-valued reflection coefficient with $|\zeta_k^i|^2$ proportional to the radar cross section (RCS) of the target. τ_k^i and $f_{D,k}^i$ are the round-trip time delay and Doppler frequency shift detected by the k-th UAV at the i-th interval, and $\phi_k^i(t)$ is the complex AWGN with zero mean and unit variance. It can be easily seen that $\tau_k^i = 2d_k^i/c_0, f_{D,k}^i = 2v_k^i f_{c,k}/c_0$, where d_k^i and v_k^i are the range and relative radial velocity between the k-th UAV and the target, and c_0 is the speed of light. It is worth noting that the UAVs intentionally detect the target within a specific area with the given parameter information, so the prior information on reflection coefficient can be known to each UAV. With the estimated distances from all UAVs, the FC can calculate the target's position by multi-lateration.

The received $r_k^i(t)$ is first down-converted to the baseband and sampled at the frequency of $f_s = N_c\Delta f$. The sample interval is $1/f_s$ and N_c time samples can be extracted from each OFDM symbol. By removing the CP and performing the discrete Fourier transform (DFT) of length N_c, a received matrix $\mathbf{Y}_k^i \in \mathbb{R}^{N_k\times M}$ for each UAV can be derived as follows, with the known $C_{k,nm}$ removed

$$\mathbf{Y}_k^i(n,m) = a_{kn}^i \zeta_k^i e^{-\mathrm{j}2\pi f_{c,kn}\tau_k^i} \cdot e^{\mathrm{j}2\pi f_{D,k}^i mT} + \mathbf{\Phi}_k^i(n,m), \tag{7}$$

where $\mathbf{\Phi}_k^i \in \mathbb{R}^{N_k\times M}$ is the matrix representation of AWGN. Its elements are independent and identically distributed (i.i.d.) complex random variables from a circular, zero-mean Gaussian distribution with variance $\sigma_{r,k}^2$, which has the same property as in (6) for constant amplitude modulation alphabets [15].

III. Problem Formulation

In this section, we present the optimization design on sensing performance improvement under communication QoS constraints. For radar, we are interested in its location estimation accuracy, which can provide meaningful benchmarks and is usually evaluated by CRLB [4]. The derivation of the CRLB for the frequency estimate in discrete-time, one-dimensional processes can be found in [42]. In this paper, the parameter vector to be estimated is defined as $\boldsymbol{\theta}^i = \left[\boldsymbol{\theta}_1^{i\,\mathrm{T}}, \boldsymbol{\theta}_2^{i\,\mathrm{T}}\right]^{\mathrm{T}} \in \mathbb{R}^{2K\times 1}$, with $\boldsymbol{\theta}_1^i = \left[\tau_1^i, \cdots, \tau_K^i\right]^{\mathrm{T}}$, and $\boldsymbol{\theta}_2^i = \left[f_{D,1}^i, \cdots, f_{D,K}^i\right]^{\mathrm{T}}$. Regarding the observation output $\mathbf{Y}_k^i$ in (7), the elements of the observation matrix are subject to the following likelihood function

$$\begin{aligned} f\left(\mathbf{Y}^i \mid \boldsymbol{\theta}^i\right) = \prod_{k\in\mathcal{K}} \prod_{n\in\mathcal{N}_k^i} \prod_{m=0}^{M-1} \frac{1}{\sqrt{2\pi\sigma_{r,k}^2}} \exp\left\{-\frac{1}{2\sigma_{r,k}^2}\right. \\ \left. \times \left|\mathbf{Y}_k^i(n,m) - a_{kn}^i \zeta_k^i e^{-\mathrm{j}2\pi f_{c,kn}\tau_k^i} e^{\mathrm{j}2\pi f_{D,k}^i mT}\right|^2\right\}. \end{aligned} \tag{8}$$

Then, the delay and Doppler shift can be estimated from the joint log-likelihood function $\ln f\left(\mathbf{Y}^i \mid \boldsymbol{\theta}^i\right)$ by using the periodogram-based estimation algorithms or maximum likelihood estimation, which have low computational complexity and good performance. The FIM of $\boldsymbol{\theta}^i$ can be written as

$$\mathbf{J}(\boldsymbol{\theta}^i) = \begin{bmatrix} \mathbf{J}\left(\boldsymbol{\theta}_1^i, \boldsymbol{\theta}_1^i\right) & \mathbf{J}\left(\boldsymbol{\theta}_1^i, \boldsymbol{\theta}_2^i\right) \\ \mathbf{J}\left(\boldsymbol{\theta}_1^i, \boldsymbol{\theta}_2^i\right)^{\mathrm{T}} & \mathbf{J}\left(\boldsymbol{\theta}_2^i, \boldsymbol{\theta}_2^i\right) \end{bmatrix}. \tag{9}$$

According to the FIM of $\boldsymbol{\theta}^i$, the CRLB on delay and Doppler shift estimation can be calculated as

$$\begin{aligned} \mathrm{CRLB}\left(\tau_k^i\right) &= \frac{32\pi(2M-1)}{M(M+1){c_0}^2\sigma_{\mathrm{RCS}}} \frac{\left(d_k^i\right)^4 \sigma_{r,k}^2}{P_k^i}, \\ \mathrm{CRLB}\left(f_{D,k}^i\right) &= \frac{192\pi f_{c,k}^2}{M(M-1)^2T^2{c_0}^2\sigma_{\mathrm{RCS}}} \frac{\left(d_k^i\right)^4 \sigma_{r,k}^2}{P_k^i}. \end{aligned} \tag{10}$$

Then, to obtain the CRLB matrix of the target's location, we are mainly interested in the first subvector to achieve the

[4]The corresponding practical error variances can be minimized by optimizing the CRLBs, which is known to be asymptotically tight to the MSE of the maximum likelihood estimator at high signal-to-noise ratio (SNR) and is validated in [16].

distances between the UAVs and the target. For simplicity, the EFIM $\mathbf{J}_e\left(\boldsymbol{\theta}_1^i\right)$ is introduced to measure $\boldsymbol{\theta}_1^i$ [39].

Lemma 1. *Define the parameter vector of interest to be estimated as* $\boldsymbol{\omega}^i = \left[\, x_0^i, y_0^i\right]^T$*, the EFIM* $\mathbf{J}\left(\boldsymbol{\omega}^i\right)$ *of the target location is*

$$\mathbf{J}\left(\boldsymbol{\omega}^i\right) = \mathbf{Q}_i \mathbf{J}_e\left(\boldsymbol{\theta}_1^i\right) \mathbf{Q}_i^{\mathrm{T}}, \tag{11}$$

with $\mathbf{J}_e\left(\boldsymbol{\theta}_1^i\right)$ *and* $\mathbf{Q}_i$ *given in (36) and (37).*

Proof: See Appendix A. ■

The inverse of the EFIM matrix $\mathbf{J}\left(\boldsymbol{\omega}^i\right)$ can finally define the CRLB matrix on the target location estimation as

$$\mathbf{C}_{x,y}^i = \left\{ A_0 \sum_{k\in\mathcal{K}} P_k^i \left[\begin{array}{cc} g_{k_{11}}^i & g_{k_{12}}^i \\ g_{k_{21}}^i & g_{k_{22}}^i \end{array} \right] \right\}^{-1}, \tag{12}$$

where $A_0 = \frac{M(M+1)\sigma_{\mathrm{RCS}}}{8\pi(2M-1)}$, and

$$\begin{cases} g_{k_{11}}^i = \frac{\left(x_0^i - x_k^i\right)^2}{{d_k^i}^6 \sigma_{r,k}^2}, \\ g_{k_{12}}^i = g_{k_{21}}^i = \frac{\left(x_0^i - x_k^i\right)\left(y_0^i - y_k^i\right)}{{d_k^i}^6 \sigma_{r,k}^2}, \\ g_{k_{22}}^i = \frac{\left(y_0^i - y_k^i\right)^2}{{d_k^i}^6 \sigma_{r,k}^2}. \end{cases} \tag{13}$$

It can be observed that the CRLB for location estimation for the multi-UAV ISAC system has a similar format as that in [43][44]. The trace of $\mathbf{C}_{x,y}^i$ accounts for a lower bound on the sum of the MSEs for the estimation on target location $\boldsymbol{\omega}^i$, i.e., $\mathrm{tr}\left(\mathbf{C}_{x,y}^i\right) \le \left(\sigma_x^i\right)^2 + \left(\sigma_y^i\right)^2$, where $\left(\sigma_x^i\right)^2$ and $\left(\sigma_y^i\right)^2$ are the MSEs of the location estimation on x_0^i and y_0^i. Thus, the localization performance of the UAVs can be evaluated and optimized by minimizing the trace of the CRLB matrix.

Let us consider the scenarios that require high sensing performance (e.g., autonomous vehicles), where the design degree of freedom (DoF) for improving the communication capacity is limited. Therefore, the objective in this paper is to minimize the estimation MSE with the guaranteed QoS of each UAV. The joint sensing and communication performance mainly depend on the allocated power and bandwidth to each UAV, the number of OFDM symbols in each pulse, and the bearing angle and distance between each tracking UAV and the target. All these parameters are incorporated into the elements of the CRLB matrix and the constraints through vectors $\{\mathbf{q}_k^i\}$, $\mathbf{n}^i$, $\mathbf{p}^i$, and matrix $\boldsymbol{\Lambda}^i$. Based on the above analysis, the design problem of this ISAC system can be formulated as

$$(\mathbf{P1}) \quad \min_{\{\mathbf{q}_k^i\},\boldsymbol{\Lambda}^i,\mathbf{n}^i,\mathbf{p}^i} \quad \mathrm{tr}\left(\mathbf{C}_{x,y}^i\right) \tag{14}$$

$$\text{s.t.} \quad R_{c,k}^i \ge \eta_c, \quad \forall k \in \mathcal{K}, \tag{14a}$$

$$\mathbf{1}^{\mathrm{T}}\mathbf{n}^i = N_c, \tag{14b}$$

$$\mathbf{1}^{\mathrm{T}}\mathbf{p}^i \le P_T, \tag{14c}$$

$$P_k^i \ge P_{\min}, \quad \forall k \in \mathcal{K}, \tag{14d}$$

$$\left\|\mathbf{q}_k^i - \mathbf{q}_k^{i-1}\right\| \le v_{\max}\delta_t, \quad \forall k \in \mathcal{K}, \tag{14e}$$

$$\left\|\mathbf{q}_m^i - \mathbf{q}_n^i\right\| \ge d_{\min}, \quad \forall m,n \in \mathcal{K}, \tag{14f}$$

$$\left\|\boldsymbol{\omega}^{i-1} - \mathbf{q}_k^i\right\| \ge d_{\min}, \quad \forall k \in \mathcal{K}, \tag{14g}$$

$$(3),$$

where constraint (14a) represents the throughput requirements of the UAVs which also guarantees fairness to all users, constraints (14c) and (14d) limit the power allocation, and (14f) and (14g) are the anti-collision constraints. η_c is the minimum communication rate, $P_{\min}$ is a minimum power which enables each UAV to communicate with BSs and localize the target, $v_{\max}$ is the maximum velocity of each UAV, δ_t is the unit flight time slot, and $d_{\min}$ denotes the minimum distance to keep UAVs from collision.

Problem $(\mathbf{P1})$ is highly challenging to solve due to the following reasons: 1) the objective function with a fractional form is complicated and non-convex; 2) the variables $\{\mathbf{q}_k^i\}$, $\mathbf{n}^i$, and $\mathbf{p}^i$ are coupled; 3) the constraints on $\boldsymbol{\Lambda}^i$ and $\mathbf{n}^i$ imply a mixed-integer programming.

IV. Proposed Solutions

In this section, we solve the problem $(\mathbf{P1})$ by optimizing the UAV trajectories, user association, and resource allocation to minimize the localization CRLB. As the problem is generally intractable, we propose the APRA algorithm based on alternating optimization, pattern search, Hungarian algorithm, and SCA to make it tractable.

A. UAV Path Planning and User Association

Fixing $\bar{\mathbf{p}}^i$, $\bar{\boldsymbol{\Lambda}}^i$, and $\bar{\mathbf{n}}^i$, the sub-problem of optimizing $\left\{\mathbf{q}_k^i\right\}$ in problem $(\mathbf{P1})$ can be written as

$$(\mathbf{P2.1}) \quad \min_{\left\{\mathbf{q}_k^i\right\}} \quad \mathrm{tr}\left(\mathbf{C}_{x,y}^i\right) \tag{15}$$

$$\text{s.t.} \quad (14e), (14f), (14g).$$

To simplify the problem, we define

$$x_k^i - \hat{x}_0^i = d_k^i \cos\psi_k^i, \tag{16a}$$

$$y_k^i - \hat{y}_0^i = d_k^i \sin\psi_k^i. \tag{16b}$$

As shown in Fig. 4, d_k^{i-1} denotes the distance from the k-th UAV to the target at the (i-1)-th interval, and it can be derived that $\beta_k^{i-1} = \arcsin\frac{r_2}{d_k^{i-1}}$, $\psi_k^i = \arccos\frac{x_k^i - \hat{x}_0^i}{d_k^i}$ with $y_k^i - \hat{y}_0^i \ge 0$, and otherwise, $\psi_k^i = 2\pi - \arccos\frac{x_k^i - \hat{x}_0^i}{d_k^i}$.

Lemma 2. *To minimize the CRLB for target location estimation, the problem (**P2.1**) can be reduced to*

$$(\mathbf{P2.2}) \quad \min_{\boldsymbol{\psi}^i} \quad \mathrm{tr}\left(\tilde{\mathbf{C}}_{x,y}^i\right) \tag{17}$$

$$\text{s.t.} \quad \check{\psi}_k^i \le \psi_k^i \le \hat{\psi}_k^i \tag{17a}$$

$$(14f),$$

where

$$\tilde{\mathbf{C}}_{x,y}^i = \frac{1}{A_0}\left\{ \sum_{k\in\mathcal{K}} P_k^i \left[\begin{array}{cc} \frac{\cos^2\psi_k^i}{{d_{k,\min}^i}^4 \sigma_{r,k}^2} & \frac{\cos\psi_k^i \sin\psi_k^i}{{d_{k,\min}^i}^4 \sigma_{r,k}^2} \\ \frac{\cos\psi_k^i \sin\psi_k^i}{{d_{k,\min}^i}^4 \sigma_{r,k}^2} & \frac{\sin^2\psi_k^i}{{d_{k,\min}^i}^4 \sigma_{r,k}^2} \end{array} \right] \right\}^{-1}, \tag{18}$$

and

$$\left[\check{\psi}_k^i, \hat{\psi}_k^i\right] = \begin{cases} \left[\psi_k^{i-1} - \beta_k^{i-1}, \psi_k^{i-1} + \beta_k^{i-1}\right], & r_1 + r_2 \le d_k^{i-1}, \\ \left[\psi_k^{i-1} - \xi_k^{i-1}, \psi_k^{i-1} + \xi_k^{i-1}\right], & r_1 + r_2 > d_k^{i-1}, \end{cases} \tag{19}$$

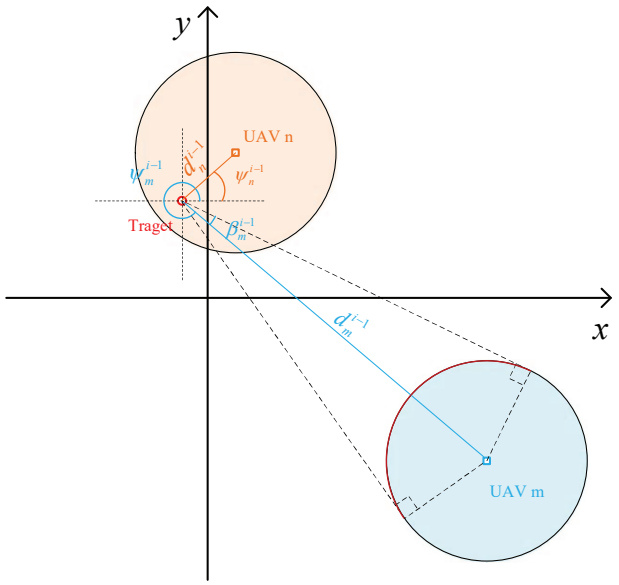

Fig. 4. Measurement model for UAV path planning analysis.

with $\xi_k^{i-1} = \arccos \frac{r_1^2+r_2^2-d_k^{i-1\,2}}{2r_1r_2}$, *and* $\boldsymbol{\psi}^i = \left[\psi_1^i, \cdots, \psi_K^i\right]^T$.

Proof: See Appendix B. ■

The objective function (17) is highly non-linear and complicated, making the problem $(\mathbf{P2.2})$ hard to solve by gradient-based optimization algorithms which are sensitive to the initial condition and liable to be trapped in a local optimum. By employing Lemma 2, the dimension and range of the feasible region can be effectively reduced. We exploit the pattern search to achieve the optimal tracking trajectory efficiently, which is computationally fast to guarantee the path planning be done in time. Once the UAVs' trajectories are obtained, the association problem for $\boldsymbol{\Lambda}^i$ can be interpreted as an assignment problem, and can be solved by the classical Hungarian algorithm. The solution for UAV path planning and user association determination is detailed in Algorithm 1.

Algorithm 1 UAV Path Planning and Association Determination

Require: $\bar{\mathbf{p}}^i$, $\bar{\mathbf{n}}^i$, $\hat{\boldsymbol{\omega}}^{i-1}$, $\{\mathbf{q}_k^{i-1}\}$, $\mathbf{u}_j$

Init: { Iteration Index $l = 0$; Mesh Tolerance ϵ_1; Feasible $\boldsymbol{\psi}_{(0)}^i$ to $(\mathbf{P2.2})$ }

Repeat

  Calculate the current values $\mathbf{d}_{\min(l)}^i$, $\check{\boldsymbol{\psi}}_{(l)}^i$, and $\hat{\boldsymbol{\psi}}_{(l)}^i$ based on (40) and (19)

  do

    one iteration of **pattern search** and achieve ${\boldsymbol{\psi}_{(l)}^i}^*$

    $\boldsymbol{\psi}_{(l+1)}^i = {\boldsymbol{\psi}_{(l)}^i}^*$

    $l = l + 1$

Until the mesh size of $\boldsymbol{\psi}^i$ is below ϵ_1

do

  Hungarian algorithm and determine ${\boldsymbol{\Lambda}^i}^*$

Output: $\{\bar{\mathbf{q}}_k^i\}$, $\bar{\boldsymbol{\Lambda}}^i$

B. Resource Allocation Scheme

1) UAV Bandwidth Allocation: Since the optimal UAV trajectories and user association are determined, it should be noted that the inappropriate bandwidth assignment may lead to an infeasible problem. Consequently, the bandwidth assignment should then be achieved before UAV transmission power optimization. The main idea is to achieve the bandwidth allocation results which can minimize the power budget satisfying the communication QoS constraints, and thus it can give priority to the design DoF for sensing accuracy.

Considering the average SNR of the subcarriers, the optimal rate-power allocation for the k-th UAV is to transmit equal number of bits on each subcarrier. Minimizing the communication power budget means minimizing the throughput, bringing it as close as possible to the threshold value η_c. Then, the required minimum power consumption to satisfy the communication QoS can be calculated as

$$\mathbf{p}_{c,\min}^i(k) = \sigma_{c,j}^2 (2^{\frac{\eta_c}{N_k^i \Delta f}} - 1) / \left|h_{kj}^i\right|^2. \tag{20}$$

The corresponding bandwidth allocation problem can be summarized as

$$(\mathbf{P3.1}) \quad \min_{\mathbf{N}^i} \quad \mathbf{1}^{\mathrm{T}} \mathbf{p}_{c,\min} \quad \text{s.t.} \quad (14a). \tag{21}$$

With the fixed $\{\bar{\mathbf{q}}_k^i\}$ and $\bar{\boldsymbol{\Lambda}}^i$, an appropriate algorithm to achieve the bandwidth assignment is proposed in Algorithm 2, where the subcarrier number is iteratively updated to achieve the minimum power consumption for communication. The initial integer values for the number of subcarriers are arbitrary integers.

Algorithm 2 Iterative Algorithm for Bandwidth Allocation

Require: $\{\bar{\mathbf{q}}_k^i\}$, $\mathbf{u}_j$

Init: { Iteration Index $l = 0$; $\mathbf{n}_{(0)}^i$ }

Repeat

  for $a = 1 : A$

    $\mathbf{n}_{(l)}(a:) = \mathbf{n}_{(l-1)}^i + \mathbf{N}_\Delta(a,:)$

    Calculate the objective function value for each $\mathbf{n}_{(l)}(a,:)$ denoted by $\mathbf{p}_a$ based on (19)

  end for

  $\left[P_{(l)}^*, a^*\right]$ =argmin$\left[\mathbf{1}^{\mathrm{T}}\mathbf{p}_1, \cdots, \mathbf{1}^{\mathrm{T}}\mathbf{p}_A\right]$

  Update $\mathbf{n}_{(l+1)}^i = \mathbf{N}_\Delta(a^*,:)$

  $l = l + 1$

Until the decrement of the objective value is equal to 0

Output: $\bar{\mathbf{n}}^i$

During each iteration in Algorithm 2, one element in $\mathbf{n}_{(l)}^i$ is chosen to be reduced by 1, and the amount is then added to any of the other elements. Thus there exists $A = (A_K^2 + 1)$ possible cases in each iteration, where $A_K^2 = \frac{K!}{(K-2)!}$ and all

cases of the allocation change can be denoted by

$$\mathbf{N}_{\Delta}=\begin{bmatrix}-1 & 1 & 0 & \cdots & 0 & 0\\ -1 & 0 & 1 & \cdots & 0 & 0\\ \vdots & \vdots & \vdots & \vdots & \vdots & \vdots\\ 0 & 0 & 0 & \cdots & -1 & 1\\ 0 & 0 & 0 & \cdots & 0 & 0\end{bmatrix}, \tag{22}$$

where each row of the matrix $\mathbf{N}_{\Delta}$ represents one case of allocation change. During the l-th iteration, the change that causes the maximum power reduction can generate the optimum subcarrier allocation as $\mathbf{n}^i_{(l)}$. The algorithm is repeated until the change in power reduction in each iteration is equal to 0. Problem $(\mathbf{P3.1})$ can be easily solved by the iterative Algorithm 2, and it is also efficient throughout the UAV's flight since the values of the previous time interval can be used as the initial value of the next. The variation in bandwidth allocation between two time intervals is little, and thus the algorithm can quickly converge to an optimal solution.

2) UAV Transmission Power Allocation: With the bandwidth allocation results, the sub-problem with respect to $\mathbf{p}^i$ can be formulated. The constraint (14a) can be reduced to a lower bound constraint by calculating $\mathbf{p}^i_{c,\min}(k)$ by (20). Then, given the other fixed variables, we have the following problem for UAV transmission power optimization

$$\begin{aligned}(\mathbf{P4.1})\quad \min_{\mathbf{p}^i}\quad & \mathrm{tr}\left(\mathbf{C}^i_{x,y}\right) && (23)\\ \text{s.t.}\quad & \mathbf{p}^i(k)\geq \mathbf{p}^i_{c,\min}(k), && (23a)\\ & \text{(14c), (14d).}\end{aligned}$$

It is obvious that the objective function defined in (12) is non-convex and involves a ratio term, which should first be relaxed by non-liner fractional programming (FP) [45]. The classical *Dinkelbach's transform* is applied to decouple the numerator and the denominator of $\mathrm{tr}\left(\mathbf{C}^i_{x,y}\right)$, thereby converting the original single-radio problem into a non-convex quadratic programming (QP) problem, and then problem $(\mathbf{P4.1})$ can be reformulated as

$$\begin{aligned}(\mathbf{P4.2})\quad \min_{\mathbf{p}^i}\quad & \frac{f\left(\mathbf{p}^i\right)-\mu g\left(\mathbf{p}^i\right)}{A_0} && (24)\\ \text{s.t.}\quad & \text{(23a), (14c), (14d),}\end{aligned}$$

where

$$f\left(\mathbf{p}^i\right)={\mathbf{c}_i}^{\mathrm{T}}\mathbf{p}^i, \tag{25a}$$

$$g\left(\mathbf{p}^i\right)=\frac{1}{2}{\mathbf{p}^i}^{\mathrm{T}}\mathbf{W}^i\mathbf{p}^i, \tag{25b}$$

with $\mathbf{c}_i=\left[\frac{1}{{d^i_1}^4\sigma^2_{r,1}},\frac{1}{{d^i_2}^4\sigma^2_{r,2}},\cdots,\frac{1}{{d^i_K}^4\sigma^2_{r,K}}\right]^{\mathrm{T}}$, and $\mathbf{W}^i(n,m)=c_{nm}$. The subscript of c interprets the index of any two random-selected UAVs among the $C^2_K=\frac{K(\ K-1)}{2!}$ combinations and is calculated as

$$c_{nm}=\frac{\left[\left(x^i_0-x^i_m\right)\left(y^i_0-y^i_n\right)-\left(x^i_0-x^i_n\right)\left(y^i_0-y^i_m\right)\right]^2}{{d^i_n}^6{d^i_m}^6}. \tag{26}$$

The new auxiliary variable μ in (24) introduced by FP is updated by

$$\mu_{(l+1)}=\frac{f\left(\mathbf{p}^i_{(l)}\right)}{g\left(\mathbf{p}^i_{(l)}\right)}, \tag{27}$$

where l is the iteration index, and $\mathbf{p}^i_{(l)}$ is the value of $\mathbf{p}^i$ at the l-th iteration.

Since $\mathbf{W}^i$ is neither positive nor negative semidefinite, it can be decomposed as a difference of two positive semidefinite matrices based on eigenvalue decomposition given as

$$\mathbf{W}^i={\mathbf{H}^i}^{\mathrm{T}}\left(\mathbf{M}^i-\mathbf{N}^i\right)\mathbf{H}^i=\mathbf{W}^i_1-\mathbf{W}^i_2, \tag{28}$$

where $\mathbf{H}^i$ is the eigenvector matrix of $\mathbf{W}^i$, $\mathbf{M}^i=\mathrm{diag}\left[\lambda_1,\cdots,\lambda_l,\mathbf{0}\right]$, $\mathbf{N}^i=\mathrm{diag}\left[\mathbf{0},-\lambda_{l+1},\cdots\right]$. Obviously, the elements in $\mathbf{M}^i$ and $\mathbf{N}^i$ are positive eigenvalues and the opposite of negative eigenvalues of $\mathbf{W}^i$, respectively. Then (24) can be converted into a difference of convex functions given as

$$\mathcal{R}\left(\mathbf{p}^i\right)=\frac{1}{A_0}\left(\underbrace{\mathbf{c}^{\mathrm{T}}_i\mathbf{p}^i+\frac{\mu}{2}{\mathbf{p}^i}^{\mathrm{T}}\mathbf{W}^i_2\mathbf{p}^i}_{\mathcal{R}_1(\mathbf{p}^i)}-\underbrace{\frac{\mu}{2}{\mathbf{p}^i}^{\mathrm{T}}\mathbf{W}^i_1\mathbf{p}^i}_{\mathcal{R}_2(\mathbf{p}^i)}\right). \tag{29}$$

Based on (29), the objective function can be effectively handled by SCA technique. First, we derive the first-order Taylor expansion of $\mathcal{R}_2\left(\mathbf{p}^i\right)$, which has been proved to be a global lower bound of a convex function

$$\begin{aligned}\mathcal{R}'_2\left(\mathbf{p}^i\right)&=\mu{\mathbf{p}^i_{(l)}}^{\mathrm{T}}\mathbf{W}^i_1\mathbf{p}^i_{(l)}-\frac{\mu}{2}{\mathbf{p}^i_{(l)}}^{\mathrm{T}}\mathbf{W}^i_1\mathbf{p}^i_{(l)}\\ &\leq\mathcal{R}_2\left(\mathbf{p}^i\right).\end{aligned} \tag{30}$$

Then (24) can be replaced by its corresponding upper bound at the l-th iteration, and problem $(\mathbf{P4.2})$ can be relaxed as

$$\begin{aligned}(\mathbf{P4.3})\quad \underset{\mathbf{p}^i}{\text{minimize}}\quad & \frac{1}{A_0}\left[\mathcal{R}_1\left(\mathbf{p}^i\right)-\mathcal{R}'_2\left(\mathbf{p}^i\right)\right] && (31)\\ \text{s.t.}\quad & \text{(23a), (14c), (14d).}\end{aligned}$$

The objective function (31) is convex since it is a combination of a convex function and a linear function. Thus it can be verified that problem $(\mathbf{P4.3})$ is a convex QP problem with linear constraints, which can be efficiently solved by standard convex optimization techniques such as active set, interior point, and conjugate gradient methods or existing software toolbox such as CVX [46]. Therefore, an efficient solution for problem $(\mathbf{P4.1})$ can be achieved by successively updating the stationary point of problem $(\mathbf{P4.3})$ at each iteration, which is summarized in Algorithm 3.

C. Overall Algorithm with Computational Complexity and Convergence Analysis

The overall algorithm is summarized in this subsection, which solves problem $(\mathbf{P1})$ by alternately optimizing the problems derived in the previous subsections. Specifically, the optimal trajectories for the ISAC UAVs in each time interval are determined by pattern search and the UAV-BS association

Algorithm 3 Dinkelbach-based SCA Algorithm for Power Allocation

Require: $\{\bar{\mathbf{q}}_k^i\}$, $\bar{\mathbf{\Lambda}}^i$, $\bar{\mathbf{n}}^i$, $\hat{\boldsymbol{\omega}}^i$, $\mathbf{p}_{c,\min}^i$

Init: Iteration Index $l = 0$; Threshold ϵ_2; Feasible $\mathbf{p}_{(0)}^i$

Repeat

  Update $\mu_{(l)}$ based on (27)

  Solve the convex problem $(\mathbf{P4.3})$ by CVX, and denote the optimal solution as $\mathbf{p}_{(l)}^i$

  $l = l + 1$

Until the decrement of the objective value of $(\mathbf{P4.3})$ is below ϵ_2

Output: $\bar{\mathbf{p}}^i$

$\mathbf{\Lambda}^i$ is generated by the Hungarian algorithm. Then, the sub-carrier number allocation $\mathbf{n}^i$ is optimized by an appropriate search algorithm. Finally, a high-quality sub-optimal solution of the UAV power allocation problem is obtained by applying the SCA technique. Furthermore, during each time interval, the achieved $\left\{\mathbf{q}_{k(n)}^i\right\}$, $\mathbf{\Lambda}_{(n)}^i$, $\mathbf{n}^i{}_{(n)}$ and $\mathbf{p}_{(n)}^i$ in the n-th iteration is used as the input of the next iteration. Similarly, the achieved $\left\{\mathbf{q}_k^i\right\}$, $\mathbf{\Lambda}^i$, $\mathbf{n}^i$ and $\mathbf{p}^i$ at the i-th interval is used as the input of the next interval. At the first time interval, the initial power allocated to the UAVs is divided equally, and the initial bandwidth is arbitrary. Details of this overall algorithm are summarized in Algorithm 4.

Algorithm 4 Overall Algorithm for Solving $(\mathbf{P1})$

Require: $\hat{\boldsymbol{\omega}}^i$, $\left\{\mathbf{q}_k^{i-1}\right\}$, $\boldsymbol{u}_j$

Init: Iteration Index $n = 0$; Threshold ϵ_0; Feasible $\mathbf{p}_{(0)}^i$, $\mathbf{\Lambda}_{(0)}^i$, and $\mathbf{n}_{(0)}^i$

Repeat

  Update $\left\{\mathbf{q}_{k(n+1)}^i\right\}$ and $\mathbf{\Lambda}_{(n+1)}^i$ via Algorithm 1

  Update $\mathbf{n}_{(n+1)}^i$ via Algorithm 2

  Update $\mathbf{p}_{(n+1)}^i$ via Algorithm 3

  $n = n + 1$

Until the decrement of $\mathrm{tr}\left(\mathbf{C}_{x,y}^i\right)$ is below ϵ_0

Output: $\mathbf{p}^i$, $\left\{\mathbf{q}_k^i\right\}$, $\mathbf{\Lambda}^i$, $\mathbf{n}^i$

The overall computational complexity of the proposed algorithm is linear with the number of iterations. Therefore, we mainly focus on the deterministic cost per iteration for the convenience of analysis. For the pattern search based UAV path planning optimization, the complexity is $\mathcal{O}(\epsilon_1^{-1}K)$. The computational cost of both user association and bandwidth allocation is linear with $\mathcal{O}(K)$. For UAV power allocation, the complexity of the reformulated problem $(\mathbf{P4.3})$ solved by the Dinkelbach-based SCA algorithm is $\mathcal{O}(K^{3.5})$. To conclude, the total complexity is polynomial over K.

The convergence of Algorithm 4 is stated by the following lemma.

Lemma 3. *The proposed overall algorithm is convergent.*

Proof: See Appendix C. ■

TABLE I
SIMULATION PARAMETERS

Parameter	Value	Parameter	Value
γ_0	-50 dB	P_T	0 dB
f_c	2.44 GHz	$P_{\min}$	-20 dB
Δf	15 kHz	N_c	1024
H	100 m	K	3
$d_{\min}$	3 m	$v_{\max}$	30 m/s
$\sigma_{c,k}^2/\sigma_{r,k}^2$	-110 dBw	σ_{RCS}	-10 dBsm
M	5	$\tilde{\alpha}$	2

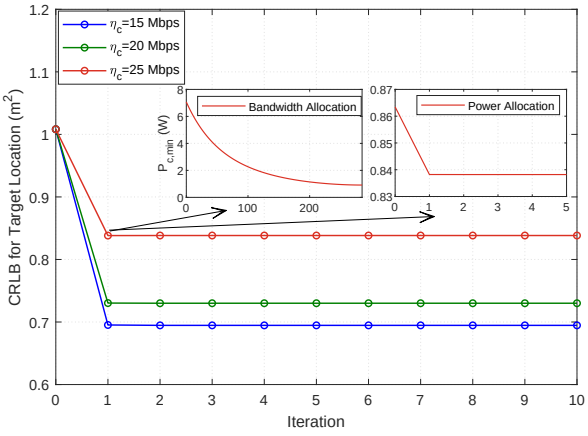

Fig. 5. Convergence of the overall algorithm with different communication constraints; the insets depict the convergence of Algorithm 2 for bandwidth allocation (left) and Algorithm 3 for power allocation (right) with $\eta_c = 25$ Mbps.

V. NUMERICAL RESULTS

In this section, the effectiveness of our proposed APRA algorithm is evaluated by numerical simulations in the ISAC scenario. Without loss of generality, the micro BSs are uniformly distributed with distance of 60 m in the considered area. The detailed simulation parameters are listed in Table I, where the UAV's altitude is according to the Federal Aviation Administration regulation [47]. The initial geometric distributions of the UAVs are set as $\mathbf{q}_1^0 = [0, 0]$, $\mathbf{q}_2^0 = [40, 0]$, and $\mathbf{q}_3^0 = [-20, 200]$, and the UAVs are constrained to keep safety distance of $d_{\min}$ m from each other. Considering that the duration of each interval in the proposed ISAC frame structure is 1 ms, we take an observation interval as 100 ms for the purpose of analysis in the following simulations.

A. Performance within One Observation Interval

First, we analyze the convergence of the proposed APRA algorithm within the first observation interval. The proposed algorithm is based on the alternating optimization approach by solving three sub-problems. Therefore, the convergence of the overall algorithm along with the convergence for the resource allocation algorithms are shown respectively in Fig. 5. Note that the overall convergence can be obtained in only a few iterations since the objective value is monotonically decreased

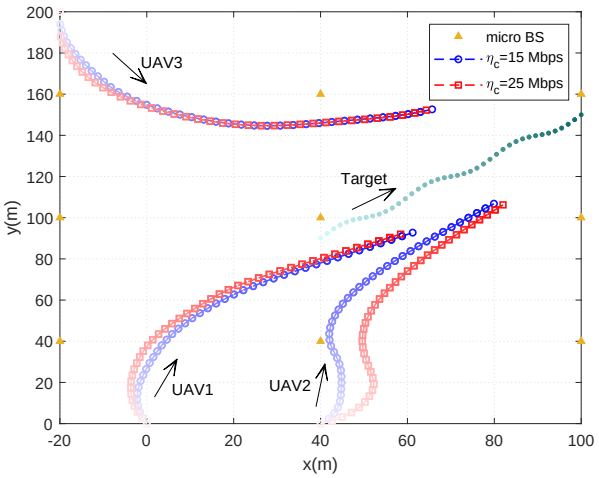

Fig. 6. The cooperative tracking trajectories of the UAVs with $\eta_c = 15$ Mbps and $\eta_c = 25$ Mbps.

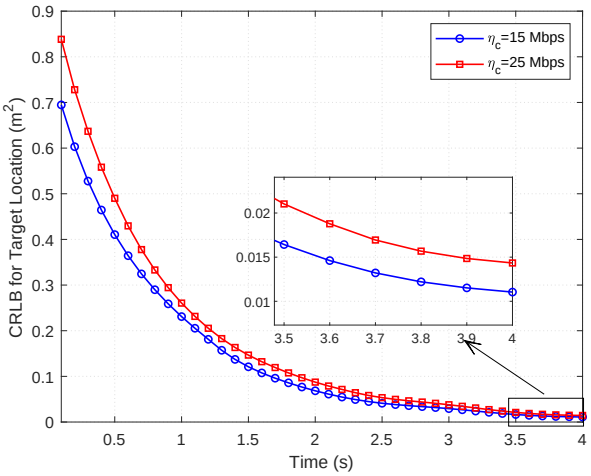

Fig. 7. Comparison with different communication constraints in terms of the improvement in $\sigma_{x,y}^2$ versus time.

as the outer iteration index rises, and the convergence for the Dinkelbach-based SCA algorithm for power allocation is also fast. Recall that the tracking performance depends on the improvements in the CRLB, which is derived as $\sigma_{x,y}^2$ in (12). Therefore, the localization performance comparison for different communication QoS constraints is also demonstrated within this observation interval. As expected, compared to the cases with stricter throughput constraints, the lower CRLB on target location estimation can be achieved with $\eta_c = 15$ Mbps. The curves show the performance trade-off between localization accuracy and throughput threshold, which is mainly dependent on the resource allocation scheme and path planning, and the principle will be elaborated further in the following subsection.

B. Performance across Observation Intervals

The simulation is then conducted over 40 consecutive observation intervals to analyze the tracking performance of this dynamic ISAC network. Based on the proposed algorithm, the optimized variables $\{\mathbf{q}_k^i\}$, $\mathbf{\Lambda}^i$, $\mathbf{n}^i$ and $\mathbf{p}^i$ are updated as the input to the next interval.

Given the pre-designed target path, Fig. 6 depicts the trajectories of the cooperative tracking UAVs achieved by our proposed algorithm, with the throughput requirement set as $\eta_c = 15$ Mbps and $\eta_c = 25$ Mbps. It is worth noting that all the tracking UAVs approach the target to improve localization accuracy as time proceeds forward. Specifically, both UAV2 and UAV3 continuously approach the target within 4 s, so as to get better localization performance. As for UAV1, it flies far away from the target at the very beginning, and actually this seemingly abnormal behavior improves the performance from the perspective of angular spread, for the reason that the localization performance is also reliant on the geometric spread of all UAVs.

As illustrated in Fig. 7, the cooperative UAV network can significantly increase the localization performance than radars with fixed deployment by permitting a continuous tracking of the target, showing the superiority of the dynamic configuration. In general, UAVs can achieve better localization accuracy throughout the whole tracking process with $\eta_c = 15$ Mbps than $\eta_c = 25$ Mbps. Moreover, the gap is gradually decreased with the growth of time, since the path planning can make up for the weakness of insufficient DoF for resource allocation.

As shown in Fig. 8, it is obvious that the allocation variations among the observation intervals are more severe with lower throughput requirements. Under the constraint of total power budget, more strict communication QoS guarantee means that the residual power for improving sensing performance is reduced. Therefore, when the communication demand is less, the minimum power per UAV required to maintain communication is decreased accordingly, and the design DoF for sensing optimization can thus be increased.

The optimality principle of the joint bandwidth and power allocation can be analyzed more comprehensively in terms of each UAV's individual ranging performance throughout the movement. First of all, it can be noticed in Fig. 9 that the performance differences between the UAVs are more evident with lower communication requirement, which is consistent with Fig. 8. Then for localization performance improvement, increasing the power can intuitively improve the performance as it potentially increases the SNR of the receiving measurements. However, the system resource is limited, and we cannot increase all UAVs' performances while satisfying various constraints and maintaining the communication QoS. Thus, a performance trade-off between the UAVs is shown in Fig. 9 (a) and (b). As we can observe from these results, in both cases, the two UAVs closer to the target are selected to be allocated more resources. Specifically, with the similar distances to the target during $t < 0.1$ s, both UAV1 and UAV2 achieve better ranging CRLB with $\eta_c = 15$ Mbps than $\eta_c = 25$ Mbps. On the contrary, UAV3 achieves worse CRLB, and the final joint localization performance with $\eta_c = 15$ Mbps is better. This is because the localization performance is significantly determined by the two UAVs with better ranging performance, which is verified and interpreted more precisely in [43]. There-

fore, UAV1 and UAV2 affect the joint localization accuracy more than UAV3. Then, with the distance between UAV1 and target gradually changing later, the resource budget is reallocated using the algorithms developed in Sections III-A and III-B. UAV3 is then selected to be allocated more resources, and the ranging error of UAV1 increases correspondingly . The sacrificed resources of UAV1 are allocated to the other two closer UAVs to obtain better joint localization performance, in both cases. To conclude, the resources are allocated such that each UAV can maintain communication and sensing simultaneously, but the two that are advantageous, which have better contributions to the localization CRLB, are allocated more resources.

Finally, Fig. 10 compares the proposed scheme with three alternative benchmark schemes in terms of the localization performance with $\eta_c = 15$ Mbps. The D-optimality experimental design is the most widely used criterion which maximizes the determinant of the FIM [48]. It can first be seen that across all the observation intervals, our proposed scheme based on the derived CRLB can achieve the best localization performance. What's more, the *D-optimality criterion* scheme performs slightly worse than the *average bandwidth allocation* scheme for a period of time due to the superiority of our derived evaluation criterion. However, since the *D-optimality criterion* scheme only changes the objective function and employees our proposed APRA algorithm, it can make up the performance gap within 1.4 s, which validates the effectiveness of the proposed algorithm. As for the effect of resource allocation on localization accuracy, the scheme with *average power allocation* has the worst performance, while the scheme with *average bandwidth allocation* can achieve a similar but slightly worse performance than the proposed scheme. It is consistent with the analysis in Section IV-B that power allocation is a determining factor for localization CRLB, and bandwidth allocation also affects CRLB by decreasing the minimum power for communication requirements. Furthermore, although the UAVs' final locations achieved by the derived criterion are not the closest to the target, they still achieve the best localization accuracy. To explain this phenomenon, recall that the localization performance during the tracking process is affected by many factors, such as the initial locations, angular spread, the previous trajectories of all UAVs, as well as the moving angle and speed of the target. As expected, the proposed optimization scheme significantly outperforms the other three benchmark schemes with a good stability, and the comparison will provide important insights to incorporate UAVs into the efficient ISAC system design.

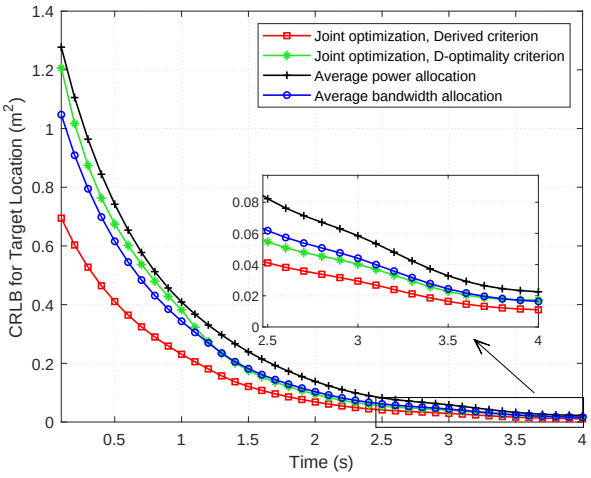

Fig. 10. Comparison of localization performance for different schemes versus time, $\eta_c = 15$ Mbps.

VI. Conclusion

This paper studied the CRLB minimization problem in a UAV-enabled ISAC system, where the UAV trajectories, user association, bandwidth, and transmission power are jointly optimized. The derived CRLB metric allows us to illustrate the impact of UAVs' dynamic trajectory and resource allocation on the sensing and communication performance trade-off. To solve the formulated problem, the minimum power budget for communication is first achieved by initializing the bandwidth allocation. Then, the pattern search, Hungarian algorithm, FP, and SCA are employed to alternately optimize the decomposed sub-problems. Numerical results validate that the proposed APRA algorithm can converge to the global value with high efficiency, and have a significant improvement in approaching the performance limit of the cooperative ISAC UAV system. Furthermore, the tracking process can make up for the weakness of insufficient DoF for resource allocation and reduce the localization performance gap caused by different throughput constraints. The proposed scheme can obviously achieve the best CRLB throughout the flight, compared to conventional techniques. In the future work, a more generalized case with 3D trajectory planning for multi-UAV-assisted system will be considered to enhance the ISAC performance. And a unified resource allocation for different sensing services, such as detection, localization, and tracking will be further designed.

Appendix A
Proof of Lemma 1

According to (9), the elements of $\mathbf{J}(\boldsymbol{\theta^i})$ can be expressed as

$$\mathbf{J}(\boldsymbol{\theta^i}) = \begin{bmatrix} \text{diag}\left(\boldsymbol{\alpha}^i\right) & \text{diag}\left(\boldsymbol{\gamma}^i\right) \\ \text{diag}\left(\boldsymbol{\gamma}^i\right) & \text{diag}\left(\boldsymbol{\beta}^i\right) \end{bmatrix}, \tag{32}$$

where $\boldsymbol{\alpha}^i = [\alpha_1^i, \cdots, \alpha_K^i]^{\mathrm{T}}$ and the elements α_k^i, γ_k^i and β_k^i are calculated as

$$\begin{cases} \alpha_k^i = \sum_{n\in\mathcal{N}_k^i} \sum_{m=0}^{M-1} \frac{\left(2\pi a_{kn}^i \left|\zeta_k^i\right| f_{c,kn}\right)^2}{\sigma_{r,k}^2}, \\ \gamma_k^i = \sum_{n\in\mathcal{N}_k^i} \sum_{m=0}^{M-1} \frac{\left(2\pi a_{kn}^i \left|\zeta_k^i\right|\right)^2 f_{c,kn} mT}{\sigma_{r,k}^2}, \\ \beta_k^i = \sum_{n\in\mathcal{N}_k^i} \sum_{m=0}^{M-1} \frac{\left(2\pi a_{kn}^i \left|\zeta_k^i\right|\right)^2 m^2 T^2}{\sigma_{r,k}^2}. \end{cases} \tag{33}$$

Then the EFIM $\mathbf{J}_e\left(\boldsymbol{\theta}_1^i\right)$ can be calculated as

$$\mathbf{J}_e\left(\boldsymbol{\theta}_1^i\right) = \mathbf{J}\left(\boldsymbol{\theta}_1^i, \boldsymbol{\theta}_1^i\right) - \mathbf{J}\left(\boldsymbol{\theta}_1^i, \boldsymbol{\theta}_2^i\right) \mathbf{J}\left(\boldsymbol{\theta}_2^i, \boldsymbol{\theta}_2^i\right)^{-1} \mathbf{J}\left(\boldsymbol{\theta}_1^i, \boldsymbol{\theta}_2^i\right)^{\mathrm{T}}, \tag{34}$$

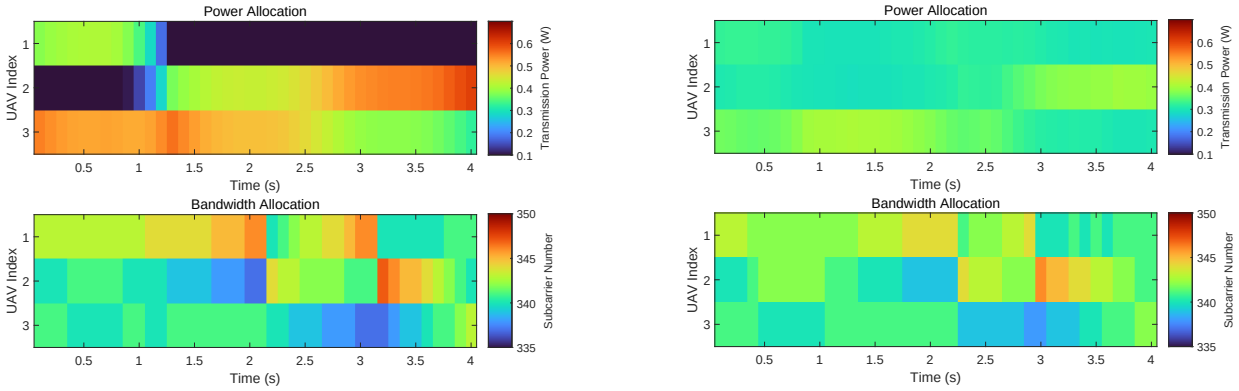

(a) $\eta_c = 15$ Mbps (b) $\eta_c = 25$ Mbps

Fig. 8. The resource allocation results versus time with different communication QoS requirements.

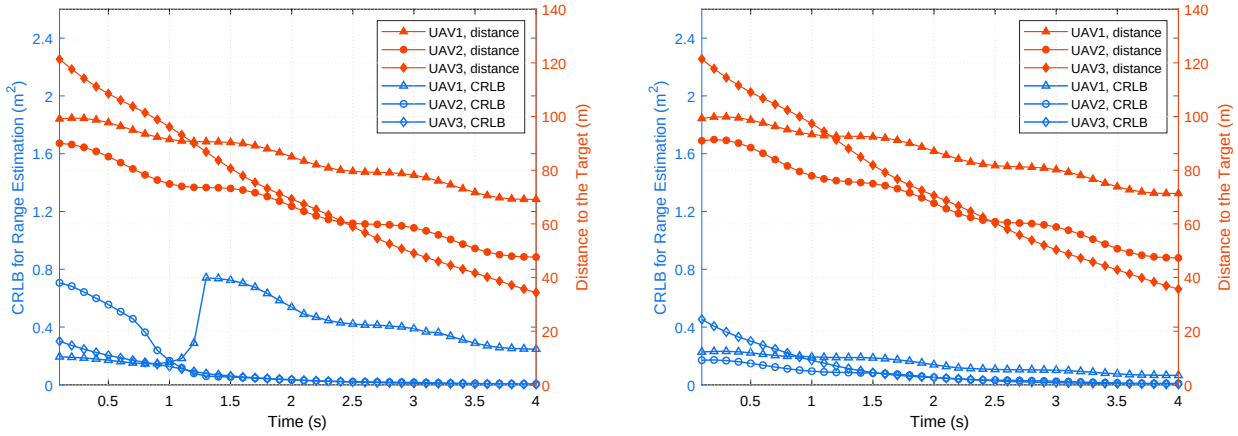

(a) $\eta_c = 15$ Mbps (b) $\eta_c = 25$ Mbps

Fig. 9. The achieved ranging performance of each UAV and the distance to the target versus time with different communication QoS requirements.

where

$$\begin{aligned}\mathbf{J}\left(\boldsymbol{\theta}_m^i, \boldsymbol{\theta}_n^i\right) &= \mathbb{E}\left\{-\Delta_{\boldsymbol{\theta}_m^i}^{\boldsymbol{\theta}_n^i} \ln f\left(\mathbf{Y}^i \mid \boldsymbol{\theta}^i\right)\right\} \\ &= \mathbb{E}\left\{\nabla_{\boldsymbol{\theta}_m^i} h\left(\boldsymbol{\theta}^i\right) \boldsymbol{\Phi}^{-1} \left(\nabla_{\boldsymbol{\theta}_n^i} h\left(\boldsymbol{\theta}^i\right)\right)^{\mathrm{H}}\right\}, \end{aligned} \quad (36)$$

and

$$h\left(\boldsymbol{\theta}^i\right) = \sum_{k\in\mathcal{K}} \sum_{n\in\mathcal{N}_k^i} \sum_{m=0}^{M-1} a_{kn}^i \zeta_k^i e^{-\mathrm{j}2\pi f_{c,kn}\tau_k^i} e^{\mathrm{j}2\pi f_{D,k}^i mT}, \quad (36)$$

with $\Delta_{\boldsymbol{\theta}_m^i}^{\boldsymbol{\theta}_n^i} = \nabla_{\boldsymbol{\theta}_m^i} \nabla_{\boldsymbol{\theta}_n^i}^T$, $\boldsymbol{\Phi}$ as the noise covariance matrix, and ∇ as the operator of the first-order partial derivative. Therefore, the elements of EFIM $\mathbf{J}_e\left(\boldsymbol{\theta}_1^i\right)$ can be calculated as $\alpha_k^i - \frac{(\gamma_k^i)^2}{\beta_k^i}$ through (34). Then $\mathbf{J}_e\left(\boldsymbol{\theta}_1^i\right)$ is achieved as

$$\mathbf{J}_e\left(\boldsymbol{\theta}_1^i\right) = \left[\mathrm{diag}\left(\frac{M(M+1)c_0^2\sigma_{\mathrm{RCS}}}{32\pi(2M-1)} \frac{P_k^i}{(d_k^i)^4\sigma_{r,k}^2}\right)\right], \quad (37)$$

by $\alpha_k^i = \frac{Mc_0^2\sigma_{\mathrm{RCS}}P_k^i}{16\pi(d_k^i)^4\sigma_{r,k}^2}$, $\gamma_k^i \approx \frac{M(M-1)Tc_0^2\sigma_{\mathrm{RCS}}P_k^i}{32\pi(d_k^i)^4\sigma_{r,k}^2 f_{c,k}}$, and $\beta_k^i \approx \frac{M(M-1)(2M-1)T^2c_0^2\sigma_{\mathrm{RCS}}P_k^i}{96\pi(d_k^i)^4\sigma_{r,k}^2 f_{c,k}^2}$. The approximation $f_{c,k}$ here is proper since its generating error is analyzed to be 10^{-8} of the order of m^2 in position localization accuracy.

As the EFIM with respect to $\boldsymbol{\theta}_1^i$ is derived, $\mathbf{J}\left(\boldsymbol{\omega}^i\right)$ can be evaluated by the chain rule in [43] as $\mathbf{J}\left(\boldsymbol{\omega}^i\right) = \mathbf{Q}_i \mathbf{J}_e\left(\boldsymbol{\theta}_1^i\right) \mathbf{Q}_i^T$, where $\mathbf{Q}_i$ is the Jacobian matrix given by

$$\mathbf{Q}_i = \frac{\partial \boldsymbol{\theta}_1^i}{\partial \boldsymbol{\omega}^i} = \frac{2}{c_0} \begin{bmatrix} \frac{x_0^i - x_1^i}{d_1^i} & \cdots & \frac{x_0^i - x_K^i}{d_K^i} \\ \frac{y_0^i - y_1^i}{d_1^i} & \cdots & \frac{y_0^i - y_K^i}{d_K^i} \end{bmatrix}. \quad (38)$$

This completes the proof.

Appendix B
Proof of Lemma 2

For the fixed ψ_m^i and d_m^i $(m \in \mathcal{K}_k, \mathcal{K}_k = \{x | x \neq k \cap x \in \mathcal{K}\})$, the total MSE of location estimation can be obtained (given in (39) at the top of next page), where $\Gamma_1 = \sum_{m\in\mathcal{K}_k} \frac{P_k^i \cos^2\psi_m^i}{(d_m^i)^4\sigma_{r,m}^2}$, $\Gamma_2 = \sum_{m\in\mathcal{K}_k} \frac{P_k^i \sin^2\psi_m^i}{(d_m^i)^4\sigma_{r,m}^2}$, and $\Gamma_3 = \sum_{m\in\mathcal{K}_k} \frac{P_k^i \sin\psi_m^i \cos\psi_m^i}{(d_m^i)^4\sigma_{r,m}^2}$. Then, the first derivative of $\mathrm{tr}\left(\tilde{\mathbf{C}}_{x,y}^i\right)$ with respect to z can be derived (given in (40) at the top of next page), where $z = {d_k^i}^2$.

Therefore, $\mathrm{tr}\left(\mathbf{C}_{x,y}^{i}\right)$ can be proved to increase monotonously with d_k^i, then, the optimum MSE is achieved at $d_{k,\min}^i$ given by

$$d_{k,\min}^{i}=\begin{cases} d_k^{i-1}\cos\psi^{+}-\sqrt{r_2^2-\left(d_k^{i-1}\sin\psi^{+}\right)^2}, & r_1+r_2\le d_k^{i-1} \\ d_{\min}, & r_1+r_2>d_k^{i-1}. \end{cases} \tag{41}$$

where $\psi^{+}=\left|\psi_k^i-\psi_k^{i-1}\right|$, $r_1=d_{\min}$, and $r_2=v_{\max}\delta_t$. This completes the proof.

Appendix C
Proof of Lemma 3

First, the UAVs' locations in the $(n+1)$-th iteration are not updated unless the CRLB obtained in Algorithm 1 is lower than the current value. Therefore, we have

$$C\left(\left\{\mathbf{q}_{k(n+1)}^{i}\right\},\mathbf{n}_{(n)}^{i},\mathbf{p}_{(n)}^{i}\right)\le C\left(\left\{\mathbf{q}_{k(n)}^{i}\right\},\mathbf{n}_{(n)}^{i},\mathbf{p}_{(n)}^{i}\right), \tag{42}$$

where $C(\cdot)$ denotes the CRLB expression with the corresponding parameters. When the sub-problem of path planning is solved, the UAV-BS association is updated accordingly. Then, when solving the bandwidth allocation problem by Algorithm 2, $\mathbf{n}_{(n+1)}^{i}$ is not updated without power reduction. Thus, we have

$$C\left(\left\{\mathbf{q}_{k(n+1)}^{i}\right\},\mathbf{n}_{(n+1)}^{i},\mathbf{p}_{(n)}^{i}\right)\le C\left(\left\{\mathbf{q}_{k(n+1)}^{i}\right\},\mathbf{p}_{(n)}^{i},\mathbf{n}_{(n)}^{i}\right). \tag{43}$$

Finally, the optimal power allocation $\mathbf{p}_{(n+1)}^{i}$ asymptotically converges to a stationary point via the SCA technique. Then, we have

$$C\left(\left\{\mathbf{q}_{k(n+1)}^{i}\right\},\mathbf{n}_{(n+1)}^{i},\mathbf{p}_{(n+1)}^{i}\right)\le C\left(\left\{\mathbf{q}_{k(n+1)}^{i}\right\},\mathbf{n}_{(n+1)}^{i},\mathbf{p}_{(n)}^{i}\right). \tag{44}$$

It should also be noted that the CRLB of the target location estimation is lower-bounded by a finite value, so the non-increasing sequence $\left\{C\left(\left\{\mathbf{q}_{k(n)}^{i}\right\},\mathbf{n}_{(n)}^{i},\mathbf{p}_{(n)}^{i}\right)\right\}$ (due to the equation (41), (42)) and (43)) will converge to a finite value. This completes the proof.

References

[1] Q. Wu, J. Xu, Y. Zeng, D. W. K. Ng, N. Al-Dhahir, R. Schober, and A. L. Swindlehurst, "A comprehensive overview on 5G-and-beyond networks with UAVs: From communications to sensing and intelligence," *IEEE J. Sel. Areas Commun.*, vol. 39, no. 10, pp. 2912–2945, Oct. 2021.

[2] A. Guerra, D. Dardari, and P. M. Djuric, "Dynamic radar networks of UAVs: A tutorial overview and tracking performance comparison with terrestrial radar networks," *IEEE Veh. Technol. Mag.*, vol. 15, no. 2, pp. 113–120, Jun. 2020.

[3] A. A. Al-Habob, O. A. Dobre, S. Muhaidat, and H. Vincent Poor, "Energy-efficient data dissemination using a UAV: An ant colony approach," *IEEE Wireless Commun. Lett.*, vol. 10, no. 1, pp. 16–20, Jan. 2021.

[4] W. Feng, J. Tang, N. Zhao, Y. Fu, X. Zhang, K. Cumanan, and K.-K. Wong, "NOMA-based UAV-aided networks for emergency communications," *China Commun.*, vol. 17, no. 11, pp. 54–66, Nov. 2020.

[5] F. Liu, Y. Cui, C. Masouros, J. Xu, T. X. Han, Y. C. Eldar, and S. Buzzi, "Integrated sensing and communications: Toward dual-functional wireless networks for 6G and beyond," *IEEE J. Sel. Areas Commun.*, vol. 40, no. 6, pp. 1728–1767, Jun. 2022.

[6] X. Zhiqiang and Y. Zeng, "An overview on integrated localization and communication towards 6G," *Sci. China Inform. Sci.*, vol. 65, no. 3, pp. 1–46, Mar. 2022.

[7] M. L. Rahman, J. A. Zhang, X. Huang, Y. J. Guo, and R. W. Heath, "Framework for a perceptive mobile network using joint communication and radar sensing," *IEEE Trans. Aerosp. Electron. Syst.*, vol. 56, no. 3, pp. 1926–1941, Jun. 2020.

[8] Z. Feng, Z. Fang, Z. Wei, X. Chen, Z. Quan, and D. Ji, "Joint radar and communication: A survey," *China Commun.*, vol. 17, no. 1, pp. 1–27, Jan. 2020.

[9] R. Li, Z. Xiao, and Y. Zeng, "Beamforming towards seamless sensing coverage for cellular integrated sensing and communication," in *Proc. IEEE Int. Conf. Commun. Workshops (ICC Workshops)*, 2022, pp. 492–497.

[10] F. Morbidi and G. L. Mariottini, "Active target tracking and cooperative localization for teams of aerial vehicles," *IEEE Trans. Control Syst. Technol.*, vol. 21, no. 5, pp. 1694–1707, Sept. 2013.

[11] K. Meng, Q. Wu, J. Xu, W. Chen, Z. Feng, R. Schober, and A. L. Swindlehurst, "UAV-enabled integrated sensing and communication: Opportunities and challenges," *IEEE Wirel. Commun.*, pp. 1–9, 2023.

[12] Z. Xiao, Z. Han, A. Nallanathan, O. A. Dobre, B. Clerckx, J. Choi, C. He, and W. Tong, "Antenna array enabled space/air/ground communications and networking for 6G," *IEEE J. Sel. Areas Commun.*, pp. 1–1, Aug. 2022.

[13] F. Liu, C. Masouros, A. P. Petropulu, H. Griffiths, and L. Hanzo, "Joint radar and communication design: Applications, state-of-the-art, and the road ahead," *IEEE Trans. Commun.*, vol. 68, no. 6, pp. 3834–3862, Jun. 2020.

[14] C. Sturm and W. Wiesbeck, "Waveform design and signal processing aspects for fusion of wireless communications and radar sensing," *Proc. IEEE*, vol. 99, no. 7, pp. 1236–1259, Jul. 2011.

[15] K. M. Braun, "OFDM radar algorithms in mobile communication networks," Ph.D. dissertation, Karlsruhe Institute of Technology, 2014.

[16] S. D. Liyanaarachchi, T. Riihonen, C. B. Barneto, and M. Valkama, "Optimized waveforms for 5G-6G communication with sensing: Theory, simulations and experiments," *IEEE Trans. Wireless Commun.*, vol. 20, no. 12, pp. 8301–8315, Dec. 2021.

[17] L. Gaudio, M. Kobayashi, B. Bissinger, and G. Caire, "Performance analysis of joint radar and communication using OFDM and OTFS," in *Proc. IEEE Int. Conf. Commun. Workshops (ICC Workshops)*, 2019, pp. 1–6.

[18] C. Baquero Barneto, T. Riihonen, M. Turunen, L. Anttila, M. Fleischer, K. Stadius, J. Ryynnen, and M. Valkama, "Full-duplex OFDM radar with LTE and 5G NR waveforms: Challenges, solutions, and measurements," *IEEE Trans. Microw. Theory Tech.*, vol. 67, no. 10, pp. 4042–4054, Oct. 2019.

[19] M. Temiz, E. Alsusa, and M. W. Baidas, "A dual-functional massive MIMO OFDM communication and radar transmitter architecture," *IEEE Trans. Veh. Technol.*, vol. 69, no. 12, pp. 14 974–14 988, Dec. 2020.

[20] Y. Liu, G. Liao, J. Xu, Z. Yang, and Y. Zhang, "Adaptive OFDM integrated radar and communications waveform design based on information theory," *IEEE Commun. Lett.*, vol. 21, no. 10, pp. 2174–2177, Oct. 2017.

[21] S. D. Liyanaarachchi, C. B. Barneto, T. Riihonen, and M. Valkama, "Joint OFDM waveform design for communications and sensing convergence," in *Proc. IEEE Int. Conf. Commun. (ICC)*, 2020, pp. 1–6.

[22] Z. Cheng, Z. He, and B. Liao, "Hybrid beamforming design for OFDM dual-function radar-communication system," *IEEE J. Sel. Topic Signal Process.*, vol. 15, no. 6, pp. 1455–1467, Nov. 2021.

[23] X. Wang, Z. Fei, J. A. Zhang, J. Huang, and J. Yuan, "Constrained utility maximization in dual-functional radar-communication multi-UAV networks," *IEEE Trans. Commun.*, vol. 69, no. 4, pp. 2660–2672, Apr. 2021.

[24] Y. Pan, X. Da, H. Hu, Y. Huang, M. Zhang, K. Cumanan, and O. A. Dobre, "Joint optimization of trajectory and resource allocation for time-constrained UAV-enabled cognitive radio networks," *IEEE Trans. Veh. Technol.*, vol. 71, no. 5, pp. 5576–5580, May. 2022.

[25] S. Shakoor, Z. Kaleem, D.-T. Do, O. A. Dobre, and A. Jamalipour, "Joint optimization of UAV 3-D placement and path-loss factor for energy-efficient maximal coverage," *IEEE Internet Things J.*, vol. 8, no. 12, pp. 9776–9786, Jun. 2021.

[26] A. Masaracchia, L. D. Nguyen, T. Q. Duong, C. Yin, O. A. Dobre, and E. Garcia-Palacios, "Energy-efficient and throughput fair resource allocation for TS-NOMA UAV-assisted communications," *IEEE Trans. Commun.*, vol. 68, no. 11, pp. 7156–7169, Nov. 2020.

[27] L. Wu, W. Wang, Z. Ji, Y. Yang, K. Cumanan, G. Chen, Z. Ding, and O. A. Dobre, "UAV-assisted maritime legitimate surveillance: Joint trajectory design and power allocation," *IEEE Trans. Veh. Technol.*, pp. 1–6, 2023.

[28] J. Liu, F. Zeng, W. Wang, Z. Sheng, X. Wei, and K. Cumanan, "Trajectory design for UAV-enabled maritime secure communications:

$$\operatorname{tr}\left(\tilde{\mathbf{C}}_{x,y}^{i}\right)=\frac{1}{A}\frac{\left(\Gamma_1+\frac{P_k^i\cos^2\psi_k^i}{{d_k^i}^4}\right)+\left(\Gamma_2+\frac{P_k^i\sin^2\psi_k^i}{{d_k^i}^4}\right)}{\left(\Gamma_1+\frac{P_k^i\cos^2\psi_k^i}{{d_k^i}^4}\right)\left(\Gamma_2+\frac{P_k^i\sin^2\psi_k^i}{{d_k^i}^4}\right)-\left(\Gamma_3+\frac{P_k^i\sin\psi_k^i\cos\psi_k^i}{d_k^{i4}}\right)^2}, \tag{39}$$

$$\frac{\partial\operatorname{tr}\left(\tilde{\mathbf{C}}_{xy}^{i}\right)}{\partial z}=\frac{2P_k^i\left[\left(\Gamma_1\sin\psi_k^i-\Gamma_3\cos\psi_k^i\right)^2+\left(\Gamma_2\cos\psi_k^i-\Gamma_3\sin\psi_k^i\right)^2\right]z}{\left[\left(\Gamma_1\Gamma_2-\Gamma_3^2\right)z^2+P_k^i\left(\Gamma_1\sin^2\psi_k^i+\Gamma_2\cos^2\psi_k^i-2\Gamma_3\sin\psi_k^i\cos\psi_k^i\right)\right]^2}, \tag{40}$$

A reinforcement learning approach," *China Commun.*, vol. 19, no. 9, pp. 26–36, 2022.

[29] W. Wang, X. Li, M. Zhang, K. Cumanan, D. W. Kwan Ng, G. Zhang, J. Tang, and O. A. Dobre, "Energy-constrained UAV-assisted secure communications with position optimization and cooperative jamming," *IEEE Trans. Commun.*, vol. 68, no. 7, pp. 4476–4489, Jul. 2020.

[30] W. Wang, X. Li, R. Wang, K. Cumanan, W. Feng, Z. Ding, and O. A. Dobre, "Robust 3D-trajectory and time switching optimization for dual-UAV-enabled secure communications," *IEEE J. Sel. Areas Commun.*, vol. 39, no. 11, pp. 3334–3347, Nov. 2021.

[31] Y. Zhao, Z. Li, N. Cheng, B. Hao, and X. Shen, "Joint UAV position and power optimization for accurate regional localization in space-air integrated localization network," *IEEE Internet Things J.*, vol. 8, no. 6, pp. 4841–4854, Mar. 2021.

[32] S. Xu, Y. Ou, and X. Wu, "Optimal sensor placement for 3-D time-of-arrival target localization," *IEEE Trans. Signal Process.*, vol. 67, no. 19, pp. 5018–5031, Oct. 2019.

[33] S. Xu and K. Doanay, "Optimal sensor deployment for 3D AOA target localization," in *Proc. IEEE Int. Conf. Acoust. Speech Signal Process. (ICASSP)*, 2015, pp. 2544–2548.

[34] J. Gu, T. Su, Q. Wang, X. Du, and M. Guizani, "Multiple moving targets surveillance based on a cooperative network for multi-UAV," *IEEE Commun. Mag.*, Apr. 2018.

[35] F. Koohifar, A. Kumbhar, and I. Guvenc, "Receding horizon multi-UAV cooperative tracking of moving RF source," *IEEE Commun. Lett.*, vol. 21, no. 6, pp. 1433–1436, Jun. 2017.

[36] O. Esrafilian, R. Gangula, and D. Gesbert, "Three-dimensional-map-based trajectory design in UAV-aided wireless localization systems," *IEEE Internet Things J.*, vol. 8, no. 12, pp. 9894–9904, Jun. 2021.

[37] X. Chen, Z. Feng, Z. Wei, F. Gao, and X. Yuan, "Performance of joint sensing-communication cooperative sensing UAV network," *IEEE Trans. Veh. Technol.*, vol. 69, no. 12, pp. 15 545–15 556, Dec. 2020.

[38] K. Meng, Q. Wu, S. Ma, W. Chen, and T. Q. S. Quek, "UAV trajectory and beamforming optimization for integrated periodic sensing and communication," *IEEE Wireless Commun. Lett.*, vol. 11, no. 6, pp. 1211–1215, Jun. 2022.

[39] Y. Shen and M. Z. Win, "Fundamental limits of wideband localization part I: A general framework," *IEEE Trans Inf. Theory*, vol. 56, no. 10, pp. 4956–4980, Oct. 2010.

[40] M. Mozaffari, W. Saad, M. Bennis, and M. Debbah, "Unmanned aerial vehicle with underlaid device-to-device communications: Performance and tradeoffs," *IEEE Trans. Wireless Commun.*, vol. 15, no. 6, pp. 3949–3963, 2016.

[41] D. Kivanc, G. Li, and H. Liu, "Computationally efficient bandwidth allocation and power control for OFDMA," *IEEE Trans. Wireless Commun.*, vol. 2, no. 6, pp. 1150–1158, Nov. 2003.

[42] M. K. Steven, "Fundamentals of statistical signal processing," *Technometrics*, vol. 37, no. 4, pp. 465–466, 1993.

[43] H. Godrich, A. P. Petropulu, and H. V. Poor, "Power allocation strategies for target localization in distributed multiple-radar architectures," *IEEE Trans. Signal Process.*, vol. 59, no. 7, pp. 3226–3240, Jul. 2011.

[44] T. Zhao and T. Huang, "Cramer-Rao lower bounds for the joint delay-doppler estimation of an extended target," *IEEE Trans. Signal Process.*, vol. 64, no. 6, pp. 1562–1573, Mar. 2016.

[45] K. Shen and W. Yu, "Fractional programming for communication systems-part I: Power control and beamforming," *IEEE Trans. Signal Process.*, vol. 66, no. 10, pp. 2616–2630, May. 2018.

[46] M. Grant and S. Boyd, (2016). *CVX: MATLAB Software for Disciplined Convex Programming*. [Online]. Available: http://cvxr.com/cvx.

[47] Accessed: Jul. 2022. [Online]. Available: https://www.faa.gov/news/speeches/news_story.cfm?newsid=22294.

[48] D. Ucinski, *Optimal measurement methods for distributed parameter system identification*. CRC press, 2004.

Yu Pan received the B.S. degree in electronic and information engineering from Northwestern Polytechnical University, Xian, in 2017 and the Ph.D. degree in information and communication engineering from Air Force Engineering University, Xian, in 2023. She is currently a Lecturer with the School of Electronic Countermeasures, National University of Defense Technology, Hefei, China. Her current research interests include UAV communication, integrated sensing and communication, cognitive radio networks, non-orthogonal multiple access (NOMA), and convex optimization techniques.

Ruoguang Li (S'16-M'21) received his Ph.D. degree in electrical science and technology from the School of Electrical Engineering, Beijing University of Posts and Telecommunications, Beijing, China, in 2020. From 2017 to 2019, he was a visiting Ph.D. student with the Department of Electrical and Computer Engineering, University of Houston, TX, USA. He is currently a Post-Doctoral Fellow with the National Mobile Communications Research Laboratory, Southeast University, Nanjing, China. His current research interests include integrated sensing and communication, resource allocation, and distributed networking.

Xinyu Da received the B.S. degree in Xidian University, the M.S. degree in communication and electronic system from Air and Missile Defense College, and the Ph.D. degree from School of Marine Science and Technology, Northwestern Polytechnical University in 1983, 1988 and 2007, respectively. He was working as the professor in Information and Navigation College, Air Force Engineering University till 2020. He is currently the vice-president with Yango University, and the president with the College of Artificial Intelligence. He has been in charge of many projects, including the National Natural Science Foundation of China and the Natural Science Foundation of Shaanxi Province. His research interests include satellite communications, signal processing, cognitive radio networks and physical layer security.

Hang Hu received his B.S. degree in Telecommunications Engineering from Xidian University, Xian, China in 2010, the M.S. degree and Ph. D degree in Information and Communications Engineering at College of Communications Engineering, PLA University of Science and Technology, Nanjing, China, in 2012 and 2016, respectively. He is now an associate professor at College of Information and Navigation, Air Force Engineering University in Xian, China. He has been in charge of many projects, including those with the National Natural Science Foundation of China and the Natural Science Foundation of Shaanxi Province. His current research interests include intelligent military communication technology, space-air communication network and green communications.

Miao Zhang (S'18, M'20) received his B.Sc. degree in Optical Information Science and Technology from Guizhou University, Guiyang, China, M.Sc. in Communications and Signal Processing from the University of Newcastle upon Tyne, Newcastle upon Tyne, UK, and the PhD from the University of York, York, UK in 2011, 2015 and 2020, respectively. He is currently an associate professor at the School of Information Science and Engineering, Chongqing Jiaotong University, Chongqing, China. His research interests are convex optimization techniques, intelligent reflecting surface assisted wireless networks, physical layer security and machine learning techniques for wireless communications.

Dong Zhai received his B.S. degree in Electronic Information Science and Technology from Shanxi University, Taiyuan, China, in 2016, and the M.S. degree in Information and Communication Engineering and the Ph.D degree in Cyberspace Security from Air Force Engineering University, Xian, China, in 2018 and 2022, respectively. He is currently a lecturer at Equipment Management and Unmanned Aerial Vehicle Engineering School, Air Force Engineering University, China. His research interests include UAV networking and network security.

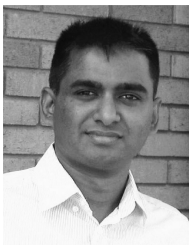

Kanapathippillai Cumanan (Senior Member, IEEE) received the B.Sc. degree (with first class Hons.) in electrical and electronic engineering from the University of Peradeniya, Sri Lanka, in 2006 and the Ph.D. degree in signal processing for wireless communications from Loughborough University, Loughborough, U.K., in 2009. He is currently a Senior Lecturer with the School of Physics, Engineering and Technology, University of York, York, U.K. From March 2012 to November 2014, he was a Research Associate with the School of Electrical and Electronic Engineering, Newcastle University, Newcastle upon Tyne, U.K. Prior to this, he was with the School of Electronic, Electrical and System Engineering, Loughborough University, Loughborough, U.K. In 2011, he was an Academic Visitor with the Department of Electrical and Computer Engineering, National University of Singapore, Singapore. From January 2006 to August 2006, he was a Teaching Assistant with the Department of Electrical and Electronic Engineering, University of Peradeniya, Sri Lanka. He has authored or coauthored more than 100 journal articles and conference papers. His research interests include non-orthogonal multiple access (NOMA), cell-free massive MIMO, Open-RAN, WiFi networks, physical layer security, convex optimization techniques, and resource allocation techniques. He is currently an Associate Editor for IEEE JSAC-MACHINE LEARNING IN COMMUNICATIONS AND NETWORKS, IEEE WIRELESS COMMUNICATIONS LETTERS and IEEE OPEN JOURNAL OF COMMUNICATIONS SOCIETY. Dr. Cumanan was the recipient of an Overseas Research Student Award Scheme (ORSAS) from Cardiff University, Wales, U.K., where he was a Research Student between September 2006 to July 2007.

Octavia A. Dobre (Fellow, IEEE) received the Dipl. Ing. and Ph.D. degrees from the Polytechnic Institute of Bucharest, Romania, in 1991 and 2000, respectively. Between 2002 and 2005, she was with the New Jersey Institute of Technology, USA. In 2005, she joined Memorial University, Canada, where she is currently a Professor and Canada Research Chair Tier 1. She was a Visiting Professor with Massachusetts Institute of Technology, USA and Universit de Bretagne Occidentale, France. Her research interests encompass wireless communication and networking technologies, as well as optical and underwater communications. She has (co-)authored over 450 refereed papers in these areas. Dr. Dobre serves as the Director of Journals of the Communications Society. She was the inaugural Editor-in-Chief (EiC) of the IEEE Open Journal of the Communications Society and the EiC of the IEEE Communications Letters. She also served as General Chair, Technical Program Co-Chair, Tutorial Co-Chair, and Technical Co-Chair of symposia at numerous conferences. Dr. Dobre was a Fulbright Scholar, Royal Society Scholar, and Distinguished Lecturer of the IEEE Communications Society. She obtained Best Paper Awards at various conferences, including IEEE ICC, IEEE Globecom, IEEE WCNC, and IEEE PIMRC. Dr. Dobre is an elected member of the European Academy of Sciences and Arts, a Fellow of the Engineering Institute of Canada, and a Fellow of the Canadian Academy of Engineering.